Fungateria

Deliverable 11.1 / v1
Design and hardware implementation of initial digital twin prototype (DTP)

Project Number: 101071145

Project Acronym: FUNGATERIA

Project title: Enlisting synthetic fungal-bacteria consortia to produce multi-cellular mycelium-based ELMs with computational capability

Project start: 01 November 2022

Project duration: 48 months

European Innovation Council

Fungateria

DELIVERABLE FACTSHEET

Project Acronym | Number		FUNGATERIA | 101071145	
Deliverable Title:	Design and hardware implementation of initial digital twin prototype (DTP)		
Deliverable Description:	This deliverable reports on the design and hardware implementation of an initial Digital Twin Prototype (DTP) using and an accumulation of modelling methods to mimic the production and electrical behavior of ELMs		
Keywords:	Digital Twin Prototype, Cellular Automata, FPGA, Memristor		
Due Date:	April 2024	**Date of submission:**	30 April 2024
Month of Project:	M18	**Version/Status:**	v1
Dissemination level:	PU - Public	**Dissemination type:**	R — Document, report
Report leader:	DUTH	**Related WP task:**	T11.1
Editor(s):	DUTH		
Partner Contributions:	DUTH, KADK, UWE		
Final review and approval:	DUTH		

Document change history		
Date	**Authors**	**Description**
30 April 2024	DUTH	Initial version

PROJECT CONSORTIUM

	Name	Short Name	Country
1.	DET KONGELIGE DANSKE KUNSTAKADEMIS SKOLER FOR ARKITEKTUR, DESIGN OG KONSERVERING	KADK	DK
2.	VRIJE UNIVERSITEIT BRUSSEL	VUB	BE
3.	UNIVERSITEIT GENT	UGent	BE
4.	UNIVERSITEIT UTRECHT	UU	NL
5.	UNIVERSITETET I OSLO	UIO	NO
6.	UNIVERSITY OF THE WEST OF ENGLAND, BRISTOL	UWE	UK
7.	DEMOCRITUS UNIVERSITY OF THRACE	DUTH	GR

The FUNGATERIA project has received funding from the European Union's HORIZON-EIC-2021-PATHFINDER CHALLENGES programme under grant agreement No. 101071145

Co-funded by the European Union

European Innovation Council

Fungateria

EXECUTIVE SUMMARY

Engineered Living Materials (ELMs), particularly those based on fungal mycelium, represent a novel class of materials inspired by living organisms. These mycelium-based ELMs offer a sustainable solution to the escalating societal challenges posed by human-induced environmental disruption, resource scarcity, and increasing material demands. They are distinguished by their low-cost manufacturing process, natural ubiquity, and significant environmental advantages, including biodegradability. However, due to the complex biological mechanisms they encompass, their environmental sensitivity, the slow supply chain and regulations, these materials present significant challenges for reproduction. For the researchers and engineers to accurately predict growth patterns, optimize conditions for mycelial ELM development, and assess potential applications, a digital twin would be advantageous. Digital twins, particularly those integrating novel electrical circuitry, emerge as an optimal solution. This is due to their inherent physical and mathematical intricacies, which enable a more profound comprehension of the underlying mechanisms of the models they represent.

In this context, to effectively design a digital twin of the Engineered Living Materials (ELMs), it is crucial to select a modeling framework that can be easily ported into hardware while also taking full advantage of the available resources. Cellular Automata (CAs) have been strategically chosen for this task due to their robust ability to simulate complex systems, as well as being scalable, modular, and showcasing massive parallelism. In this framework, CAs are specifically utilized to create a detailed grid that models the reaction-diffusion processes, providing a dynamic mapping of both the electrical and morphological activities of the ELMs. This modeling approach ensures that the ELM behavior is captured with high fidelity. Leveraging this hardware-compatible modeling framework has enabled the successful implementation of a prototype on a Field-Programmable Gate Array (FPGA). With the FPGA Digital Twin prototype in place the prototype custom circuits have been designed that can emulate the initial electrical and morphological activity of the ELMs.

More specifically, we introduce a comprehensive mycelium-based ELM framework that incorporates reaction-diffusion processes and the modeling tool of Cellular Automata (CAs). This framework successfully simulates the ELM's growth mechanisms and closely resembles the mycelium's biological structure, through the exploitation of the reaction-diffusion activator-suppressor system. Furthermore, an augmented 3D version is presented that enhances the realism of our findings and strives to provide a deeper understanding of such materials. At the same time, digital twins with advanced electrical circuit integration are particularly effective, providing deep insights into the physical and mathematical aspects of these materials. Following up the CA implementation, the high-fidelity simulation of ELM behaviors and the successful prototype implementation on a Field-Programmable Gate Array (FPGA) is investigated, making a significant step towards practical applications of mycelial ELMs. With the FPGA Digital Twin prototype in place, the prototype custom circuits have been explored. Memristors, with their unique state transition capabilities and non-volatility, emerge as promising candidate for implementing a low-power, efficient digital twin of mycelium, especially for emulating mycelium's electrical activity, demonstrating versatility across various applications beyond conventional hardware limits. This deliverable explores the use of memristive nanoelectronic circuits to simulate the evolution of biological mycelium hyphae through propagation of electrical signals by introducing a novel computational approach, Memristive Oscillating Cellular Automaton (MOCA), to model the dynamic behavior of mycelium. The MOCA design

The FUNGATERIA project has received funding from the European Union's HORIZON-EIC-2021-PATHFINDER CHALLENGES programme under grant agreement No. 101071145

Co-funded by the European Union

European Innovation Council

mirrors the activator and suppressor processes observed in reaction-diffusion systems, thus simulating mycelium tip growth and branching patterns. The simulation results demonstrate the successful propagation of oscillating signals across a MOCA grid, reflecting the biological pathways within mycelium.

The FUNGATERIA project has received funding from the European Union's HORIZON-EIC-2021-PATHFINDER CHALLENGES programme under grant agreement No. 101071145

Co-funded by the European Union

European Innovation Council

Fungateria

TABLE OF CONTENTS

1 Introduction 6
1.1 Deliverable outline 7
2 Hardware-compatible Cellular Automata framework for modelling ELMs behavior 9
2.1 Reaction-diffusion CA towards 2D and 3D simulation of mycelium-based ELMs 9
2.1.1 CA grid configuration 12
2.1.2 2D and 3D representation of the discrete reaction-diffusion process 12
2.1.3 Algorithm for implementing the mycelium-based ELM model 13
2.2 Simulation results 15
2.2.1 2D model results 15
2.2.2 3D model results 18
3 Hardware implementation of DTP with FPGA 19
3.1 System design and architecture 19
3.2 Simulation results 22
4 Towards implementation of DTP with memristive circuits 24
4.1 Memristive Oscillating Cellular Automata for ELMs emulation 24
4.2 Variability tolerance analysis 25
4.2.1 Utilized device variability 26
4.2.2 Impact of variability on oscillations 27
4.3 Simulation results on mycelium tip growth and branching 29
4.4 Electrical signal propagation in mycelium fungi with memristive circuits 31
4.4.1 Mapping mycelium grid in hardware 31
4.4.2 Simulation results 34
5 Conclusions 37
Appx. I Related work 39
Appx. II References 40

The FUNGATERIA project has received funding from the European Union's HORIZON-EIC-2021-PATHFINDER CHALLENGES programme under grant agreement No. 101071145

Co-funded by the European Union

European Innovation Council

Fungateria

1 Introduction

Engineered Living Materials (ELMs) are an emerging class of materials that combine the self-healing, regenerative, and adaptive characteristics of biological systems with the structural integrity and versatility of traditional materials science [1]. This interdisciplinary field utilizes the dynamic properties of living organisms to create materials that are robust, reliable, and capable of evolving in response to environmental changes through chemical communication, nutrient uptake, and ion exchange [2]. ELMs are primarily applied in the development of biosensors, which provide sensitive and biocompatible monitoring for health and environmental purposes [3]. They also support innovative biomaterial technologies like coatings and 3D printing [4], used in biomedical applications such as wound healing [5] and bio-therapeutic implementations [6, 7, 8]. The continual evolution of ELMs through environmental interaction highlights their revolutionary potential and versatility in various scientific and practical areas.

Mycelium, the vegetative part of fungi, is a standout choice among ELMs due to its rapid growth, sustainability, and ubiquity in nature [9]. Mycelium-based ELMs offer an eco-friendly alternative to conventional materials, significantly reducing global pollution through their biodegradability. These materials help mitigate waste accumulation, environmental contamination, and natural resource depletion while lowering manufacturing costs [10, 11]. The replication of complex biological processes by these materials offers profound insights into biological networks, furthering the study and simulation of life-like systems. Moreover, mycelium's neuron-like electrical properties enable exploration of bio-inspired unconventional computations [12], significantly contributing to a sustainable future.

However, due to their intricate mechanisms, not only at the macroscopic level where the mycelium operates as a vast and complex communication network [13], but also at the microscopic level at the mycelium's tips, known as the hyphae, which exhibits behaviors such as extension, apical and lateral branching, anastomosis, nutrient uptake, and substrate diffusion, among others [14]. These mechanisms are the exact ones that we aim to replicate using reaction-diffusion (RD) systems capable of generating fractal-like patterns akin to natural mycelium networks [15, 16]. Unlike diffusion systems, which depict growth without accounting for losses and involve individually incorporating and managing each mechanism through alterations in the corresponding equations, constituting a forced growth process, reaction-diffusion systems compensate for losses via reaction processes. This results in more spontaneous growth, offering a more natural and realistic simulation of such organisms.

Towards this direction, significant research has focused on Cellular Automata (CA) over the past decades. CA are computational models that utilize parallel processing capabilities and can act as distributed computational systems [17]. In CA, complex global phenomena emerge from the local interactions of simple, identical units. CA integrate computational power with mathematical and physical concepts to explore complex systems arranged as evolving cell grids with local interconnections [18]. A defining feature of CA models is their ability to demonstrate emergent

The FUNGATERIA project has received funding from the European Union's HORIZON-EIC-2021-PATHFINDER CHALLENGES programme under grant agreement No. 101071145

Co-funded by the European Union

European Innovation Council

behavior; this is where complex patterns and behaviors develop from simple inter-cellular rules. Additionally, the parallel computing structure inherent in CA supports a versatile and robust tool for modeling and simulating expansive and intricate systems [19, 20, 21], providing insights into these systems' dynamics that might be unattainable through other modeling techniques and methodologies.

For the researchers and engineers to accurately predict growth patterns, optimize conditions for mycelial ELM development, and assess potential applications, a digital twin would be advantageous [22]. The idea of a digital twin of mycelium is rooted in the desire to replicate the complex, adaptive, and efficient communication networks found in natural mycelium. A digital twin [23] is a virtual representation that serves as the nearly identical digital equivalent of a real-world physical object, system, or process, known as the physical twin. This model is used for practical purposes including simulation, integration, testing, monitoring, and maintenance, effectively mirroring its real-world counterpart. This approach is notably applicable to the study of mycelium [24]. On top of that, there have been relevant works at the theoretical level that can analyze the phenomenon in depth [14, 25]. In terms of plausibility, this method can provide realistic results very close to the real behavior of mycelium's evolution. Implementing an FPGA based digital twin could greatly enhance the ability to predict growth patterns, optimize development conditions, and explore potential applications for mycelial ELMs.

At the same time, digital twins, particularly those integrating novel electrical circuitry, emerge as an optimal solution due to their inherent physical and mathematical intricacies, which enable a more profound comprehension of the underlying mechanisms of the models they represent. A really promising candidate for implementing an efficient digital twin of mycelium with novel hardware is memristor. Memristors are two-terminal electrical analog components that were first theorized by L. Chua in 1971 [26], and then partially realized at HP Labs in 2008 [27]. Their primary advantage is their ability to transition between states by altering their conductance in response to applied voltage, and afterwards keeping their state. As such, their non-volatility consists of a key factor for emulating the mycelium evolution using a compact and low-power component. Numerous unconventional applications have been made use of them [28]. A few specific examples include cellular automata [29, 21], the emulation of Parkinson's Disease [30], and the recognition of characters [31], proving that they are universal components ideal to fit to a large pool of applications outperforming the conventional hardware.

1.1 Deliverable outline

In Chapter 2, a comprehensive CA-based model is introduced capable of simulating the growth characteristics of mycelium-based ELMs through reaction-diffusion processes. These processes facilitate the generation of complex patterns within a CA framework, thereby enabling substantial parallelism in our simulations in contrast to basic diffusion models that solely account for growth without incorporating any loss, rendering them less realistic compared to reaction-diffusion ones. Paragraph 2.1 describes the CAs utilized in two and three dimensions for generating complex patterns, while in paragraph 2.2, simulation results are presented to validate the hardware compatible model.

In Chapter 3, leveraging the previously described hardware-compatible CA modeling framework, along with their robust ability to simulate complex systems, as well as being scalable, modular, and

The FUNGATERIA project has received funding from the European Union's HORIZON-EIC-2021-PATHFINDER CHALLENGES programme under grant agreement No. 101071145

Co-funded by the European Union

European Innovation Council

showcasing massive parallelism has enabled the successful implementation of a prototype on a Field-Programmable Gate Array (FPGA) [32], elaborated in paragraph 3.1. In detail, a digital twin of a mycelium structure has been efficiently implemented in reconfigurable hardware, while it is the ideal hardware platform for the proposed modeling framework because of its low power consumption. This characteristic allows the FPGA to appear the most efficient solution among other hardware alternatives (such as CPUs and GPUs), as it appears the lowest energy consumption for the same evolution algorithm and computational steps. The respective simulation results are presented in paragraph 3.2 featuring deeper insights about this proposed digital twin implementation.

In Chapter 4, the emphasis is placed on using memristive nanoelectronic circuits to simulate biological mycelium's hyphae evolution. In paragraph 4.1, the notion of Memristive Oscillating Cellular Automaton (MOCA) is introduced, while in paragraph 4.2, the tentative variability of the memristive device is explored, to investigate the robustness of the core element of the proposed design. The impact of the variability to the oscillatory circuit is discussed in paragraph 4.3 to ensure the use of these structures in more complex systems for real-time efficient computing. Paragraph 4.4 presents the simulation results obtained from a MOCA grid. Lastly, paragraph 4.5 is focused on the design of a system that can replicate with efficiency the main characteristics of mycelium fungi signal propagation. In detail, the CA cell's circuit equivalent along with the respective neighbors' connections circuitry are presented supported by the results of the full circuit simulations.

The FUNGATERIA project has received funding from the European Union's HORIZON-EIC-2021-PATHFINDER CHALLENGES programme under grant agreement No. 101071145

Co-funded by the European Union

European Innovation Council

Fungateria

2 Hardware-compatible Cellular Automata framework for modelling ELMs behavior

Cellular Automata (CAs) are particularly well-suited for hardware implementation due to their inherent characteristics of simplicity, locality, and parallelism. The fundamental principle of CAs involves a grid of cells, each following simple rules based on the states of neighboring cells. This localized interaction ensures that computations are simple and highly parallelizable, which aligns perfectly with the architecture of modern hardware systems. Furthermore, the modular nature of CAs enables scalability, making it feasible to increase the complexity of the model without significant changes to the underlying hardware infrastructure. This makes CAs an optimal choice for developing high-fidelity digital twins that require both detailed simulation of processes and adaptability to evolving research needs. For this purpose, a comprehensive CA-based model is introduced capable of simulating the growth characteristics of mycelium-based ELMs through reaction-diffusion processes. These processes facilitate the generation of complex patterns within a CA framework, thereby enabling substantial parallelism in our simulations in contrast to basic diffusion models that solely account for growth without incorporating any loss, rendering them less realistic compared to reaction-diffusion ones.

2.1 Reaction-diffusion CA towards 2D and 3D simulation of mycelium-based ELMs

To accurately emulate a mycelium-based ELM, it is important to incorporate the fundamental behaviors of the mycelium. On the one hand, the ELM can be understood as an outcome of microorganisms' metabolic processes, necessitating an exploration of the bidirectional interaction between the organism and its surroundings. On the other hand, it could be perceived as a substance, emphasizing the importance of its mechanical characteristics as a critical result of the model. All in all, its behaviors could be categorized into four main categories, the metabolic processes, the transport processes, the micro-structural dynamics, and the propagation. Physically these could include hyphal extension, branching, substrate diffusion, and anastomosis [33].

(a) (b)

Fig. 1. (a) Activator-suppressor interaction, and (b) effect of suppressor on the ELM's growth (adopted from [34]*)*

The mycelium tips evolution is commonly represented through a model of biased random walk with the beginning of branching to be a random occurrence. The main dynamics that are being replicated include the tip extension and branching, anastomosis, as well as the communication with external stimuli such as the substrate uptake and depletion. These dynamics are usually represented with

The FUNGATERIA project has received funding from the European Union's HORIZON-EIC-2021-PATHFINDER CHALLENGES programme under grant agreement No. 101071145

Co-funded by the European Union

European Innovation Council

Fungateria

reaction-diffusion systems that can produce fractal structures that resemble mycelium networks [15, 16]. In this deliverable, the proposed approach comprehensively embodies these specified attributes, employing a self-organizing activator-suppressor reaction-diffusion system as its foundation [35].

Reaction-diffusion systems serve as mathematical models to elucidate the spatiotemporal variations and dynamic interactions of multiple substances, thereby facilitating the generation of intricate patterns [35] and they significantly contribute to the comprehension of biological pattern formation [36]. Furthermore, these models can also scale up to any dimension desired as they are governed by partial differential equations which are not limited to any dimensions.

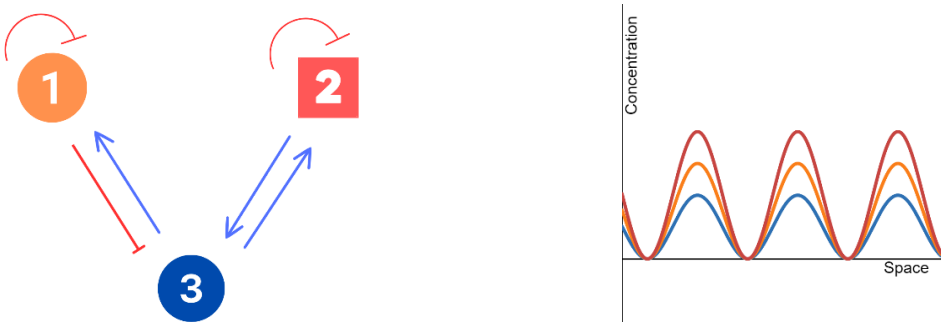

(a) (b)

Fig. 2. (a) Suppressor (1), main body (2), and activator (3) dynamics with the blue arrows to signify promotion, while the red arrows indicate suppression, and (b) concentration – space graph for the concentrations of the activator (blue), the suppressor (orange) and the main body (red) (adopted from [35]*)*

To enhance the comprehension of pattern formation, it is crucial to examine the details of the reaction-diffusion system employed [35]. This system outlines the dynamics between two key substances: the activator and the suppressor, and their influence on ELM formation. The activator encourages cell growth, and its concentration exceeding a certain threshold can initiate cell generation. On the other hand, the suppressor acts to reduce the concentration of the activator, thus having a suppressive effect. It should be highlighted that the utilized reaction-diffusion model featuring the activator and suppressor is not employed as a representation of actual chemical species, but rather as a mathematical framework to capture the system's dynamics that is general and properly fitted to reproduce the mycelium evolution. The involved abstract variables are utilized to simulate the emergent patterns and behaviors observed within the ELM bio-inspired system, distinct from directly modeling specific chemical entities.

The equations below refer to a reaction-diffusion model for bio-inspired evolution processes [34]. Herein, the activator is constrained to operate solely within the ELM, while the suppressor is allowed to function universally. This arrangement effectively restricts the growth of the activator to the confines of the ELM, thereby allowing the suppressor to direct and essentially shape the ELM's development by inhibiting the activator's undirected and unregulated expansion. In this way, the activator acts like the ELM's plasma membrane, by not only defining the borders of the ELM, but also allowing the ELM to interact with its environment in a controlled way [37]. The activator-suppressor interactions of the reaction-diffusion system utilized are summarized in Fig. 1, while the dynamics of such systems are illustrated in Fig. 2.

The FUNGATERIA project has received funding from the European Union's HORIZON-EIC-2021-PATHFINDER CHALLENGES programme under grant agreement No. 101071145

Co-funded by the European Union

European Innovation Council

Fungateria

In reaction-diffusion models, activator and suppressor pairs make it possible to simulate complex mycelial growth behaviors such as tip expansion, branching, and anastomosis. Within this framework, suppressors manage and limit growth, whereas activators promote expansion. The outward diffusion of the activator drives the extension of mycelial hyphae by effectively replicating tip extension. Branching emerges naturally, caused by the suppressor's increased concentration, which gives shape to the model by preventing the contact of the activator fronts. On the other hand, when the activator's concentration is high enough, the activator fronts merge, which is similar to anastomosis, which is when hyphal tips join together.

The mathematical expressions for the RD system are defined in the equations (1)-(4), which refer to a reaction-diffusion model for bio-inspired evolution of structures:

$$\frac{\partial \mathrm{u}}{\partial \mathrm{t}} = \nabla^2 \mathrm{u} + \zeta(\kappa \mathrm{u} + u^2 - \lambda \mathrm{uv}), \qquad where\ u \in \Omega_c \quad (1)$$

$$\frac{\partial\, \mathrm{v}}{\partial\, \mathrm{t}} = \mathrm{d}\nabla^2 \mathrm{v} + \zeta(\mu\, \mathrm{u}^2 - \mathrm{v}), \qquad where\ v \in \Omega \quad (2)$$

$$\frac{\mathrm{dc}}{\mathrm{dt}} = \zeta\, \nu\, \mathrm{c}(\mathrm{a}(\mathrm{u}) - \mathrm{c})(\mathrm{c} - 1), \qquad where\ c \in \Omega \quad (3)$$

$$a(u) = \begin{cases} \xi, & \text{if } u \geq threshold \\ \xi - \theta(u - threshold), & otherwise \end{cases} \quad (4)$$

where u and v represent the concentrations of the activator and the suppressor, respectively. On the right side of equations (1) and (2) is the initial term incorporating the Laplacian operator describing the way the solutions propagate through space, referred to as the diffusion term. Subsequently, the second term, which is a polynomial of u and v, elucidates the interaction between the solutions u and v, known as the reaction term. Equation (3) describes the derivative of the mycelium state c over time, with negative values of c to highlight the presence of a mycelial tip, while $|c|$ describes the concentration of the mycelium. Tips are formed due to the extremely high and condensed concentration of the activator in a specific area, which significantly increases c. According to equation (3), this will result in the derivative of c to be highly negative, as ξ, which will ultimately be the value of $a(u)$, is a constant selected to be smaller than 1, thus explaining the negative value of the tips. Finally, equation (4) provides the function $a(u)$, which describes the dependence of the mycelium on the activator.

It is important to highlight that v and c may assume values throughout the whole grid Ω, in contrast to u, which is restricted to values within the space delineated by Ω_C, representing the region preoccupied by cell c. Finally, ζ, κ, λ, μ and ν are all reaction parameters that affect the corresponding interactions and ultimately influence the pattern generated, while n represents the nutrient concentration of the substrate. The parameters ξ and θ directly influence $a(u)$ and enable the achievement of both positive and negative gradients in the calculation of c.

At this point, it is essential to note that these equations can fully encapsulate the desired characteristics of a reaction-diffusion model. While hardware implementation cannot fully incorporate

The FUNGATERIA project has received funding from the European Union's HORIZON-EIC-2021-PATHFINDER CHALLENGES programme under grant agreement No. 101071145

Co-funded by the European Union

European Innovation Council

Fungateria

such mathematical calculation, the described processes should be properly incorporated for the successful simulation of the ELM's growth, shape, and directionality processes.

2.1.1 CA grid configuration

In order to use the reaction-diffusion model mentioned earlier in a discrete time and space framework that allows for a lot of parallelism and a simple, modular simulation approach, a CA framework is employed. The proposed CA-based model uses a discrete square grid where each CA cell contains the values of u, v and c that are continuous. The activator is able to diffuse only within the space denoted by Ω_C. Ideally, u would diffuse radially adjacent to the mycelium, to support a more natural and realistic diffusion. However, given the computational and geometric limitations of creating a circle within a discrete grid, the activator was conditionally updated, taking into account neighbors in a circular-like fashion, as depicted in Fig. 3, where in dark blue is the center cell and in light blue its corresponding neighbors.

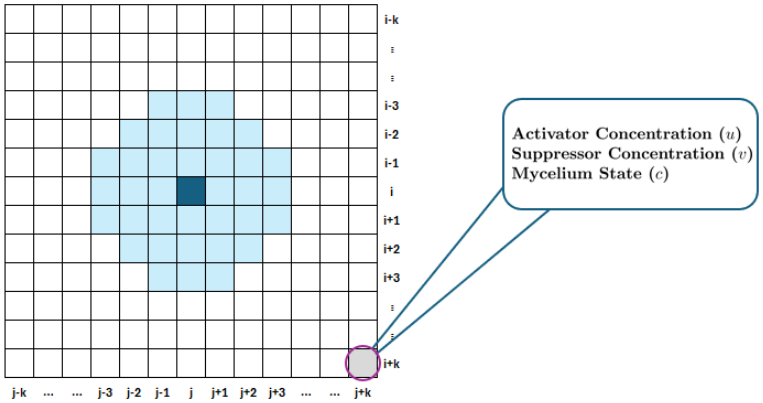

Fig. 3. Variable spaces Ω (whole grid-plane $\Pi_{i,j}$) and Ω_C. (dark and light blue colors describing the referenced cell and its neighborhood accordingly) with a depth of 3 cells in the CA grid employed. In gray, a CA cell is shown containing the three continuous values that correspond to the state equations of the activator, suppressor and mycelium.

2.1.2 2D and 3D representation of the discrete reaction-diffusion process

Before we can use the diffusion processes (equations (1) and (2)), which are usually described by partial differential equations, in a discrete CA framework, we need to use the discrete Laplacian operator. The application of this operator is equivalent to a convolution operation with a 3 x 3 kernel [38].

Furthermore, by modifying the kernel's weights, the spatial growth of the activator and the suppressor can be controlled. More specifically, it was observed that by applying two different kernels, we can achieve two different diffusion patterns in our model. The first one, which is ∇_A^2, shown in equation (6), results in a denser diffusion because of the increased central cell weight and ultimately in a more condensed mycelium. The second one, ∇_B^2, because of the increased neighbor interactions, describes a finer and more precise diffusion, resulting in the mycelium's tips. Alternating at the appropriate moments can create a more realistic growth pattern, depicting a condensed biomass at the center with emerging tips at the edges, similar to the morphology of biological fungi [39].

The FUNGATERIA project has received funding from the European Union's HORIZON-EIC-2021-PATHFINDER CHALLENGES programme under grant agreement No. 101071145

Co-funded by the European Union

European Innovation Council

Fungateria

$$\nabla_A^2 = \frac{1}{20}\begin{bmatrix}0 & 1 & 0\\ 1 & -4 & 1\\ 0 & 1 & 0\end{bmatrix}, \quad \nabla_B^2 = \frac{1}{100}\begin{bmatrix}10 & 35 & 10\\ 35 & -11 & 35\\ 10 & 35 & 10\end{bmatrix} \quad (6)$$

Moreover, we can further expand the dimensionality of the model from two dimensions, which is projected on one plane $\Pi_{i,j}$, to three dimensions, projected on three perpendicular planes: $\Pi_{i,k}$, $\Pi_{i,j}$, and $\Pi_{j,k}$. Similarly with the two dimensions, a convolution operation is performed on the planes $\Pi_{i,k}$, $\Pi_{i,j}$, and $\Pi_{j,k}$ with the three kernels $\nabla_{i,k}^2$, $\nabla_{i,k}^2$, and $\nabla_{j,k}^2$, respectively. These kernels, shown in equation (7), are introduced in [40] and are the equivalent of the 3D discrete Laplacian operator. It is noteworthy that all other parameters remain unchanged for the 3D model. Finally, it was observed that the kernel alternation didn't affect the model's growth in three dimensions, as the number of neighbors increases exponentially, rendering a small change in some of the neighbors' weights negligible.

$$\nabla_{i,k}^2 = \frac{1}{26}\begin{bmatrix}2 & 3 & 2\\ 3 & 6 & 3\\ 2 & 3 & 2\end{bmatrix}, \quad \nabla_{i,k}^2 = \frac{1}{26}\begin{bmatrix}3 & 6 & 3\\ 6 & -88 & 6\\ 3 & 6 & 3\end{bmatrix}, \quad \nabla_{j,k}^2 = \frac{1}{26}\begin{bmatrix}2 & 3 & 2\\ 3 & 6 & 3\\ 2 & 3 & 2\end{bmatrix} \quad (7)$$

It is important to note that, due to the diffusion processes that are taking place in a CA neighborhood and their resulting value being a weighted sum of all neighboring cells, both the activator and the suppressor levels can reach prohibitively high values, especially when timesteps escalate, impeding the overall system evolution. Consequently, thresholds for the activator and suppressor, denoted as $a_{\max}$ and $i_{\max}$ respectively, are introduced. As the suppressor functions like a guide for the activator, it has been determined that the system operates effectively only when the suppressor's upper limit ($i_{\max}$) exceeds the activator's one ($a_{\max}$).

2.1.3 Algorithm for implementing the mycelium-based ELM model

The algorithm detailing the model is depicted as Algorithm 1. Initially, the setting of hyperparameters (including total iterations and grid size) and the reaction-diffusion parameters takes place. Following, the concentrations of the activator, the suppressor, and the mycelium are initialized. The initialization of those three components is restricted to a small region in the center of the grid in order to observe and grasp the mycelium's growth in all possible directions. Furthermore, all three components must have an initial value: the mycelium requires the activator to grow, the activator can only propagate within the region defined by the mycelium, and the suppressor must be introduced into the system for the RD processes to function. It should be noted that the initialization within the central area is conducted randomly and given the sensitivity of reaction-diffusion systems [41], the initial randomness is propagated throughout the developing pattern with each iteration.

Moreover, the simulation incorporates a substrate that varies in its capacity to support mycelium's growth, being either more or less conducive. This is integrated as a matrix which ranges from 0 to 1, that is multiplied to the reaction part u (line 19) and either promotes or suppresses it, affecting in turn c. As a result, more fertile areas are instantiated with a higher value, while less fertile areas get a rather small non-zero value. The model also randomly introduces obstacles, such as rocks within the substrate, which are clusters of zeros inside the matrix that impede the activator's (u) development and, consequently, the growth of the mycelium in those specific areas.

The FUNGATERIA project has received funding from the European Union's HORIZON-EIC-2021-PATHFINDER CHALLENGES programme under grant agreement No. 101071145

Co-funded by the European Union

European Innovation Council

Fungateria

The CA model then initiates a loop phase where its state is continuously updated. Initially, Ω_C is established based on the neighborhood defined in Fig. 3. Then, Ω_C is iteratively updated at each simulation step to represent the confined area in which the activator can take values, resulting in the activator gradually expanding in a circular pattern. For loops in lines 9 and 10 do not iterate over the whole grid to prevent overflow, due to the considerable size of Ω_C. Next, in line 18, a kernel between ∇_A^2 and ∇_B^2 is chosen to control the diffusion of u and v. This is equivalent to a change in the CA's rule update. Subsequent processes include the conditional and unconditional update of the activator and the suppressor, respectively (lines 17-20). Following, function $a(u)$ is computed to determine the concentration of the mycelium c at each time step (lines 21-25). Lastly, concentration limiters are used to make sure that both the activator and the suppressor diffuse properly, as discussed in subparagraph 2.1.2.

Algorithm 1. Mycelium-based ELM CA Model

```
1:  grid ↤ 800
2:  iterations ↤ totalIterations
3:  ϑ, ζ, κ, λ, μ, ν, ξ, a_max, i_max, threshold ↤ initialize
4:  u, v, c ↤ rand(size(10))
5:  substrate ↤ rand(size(grid))
6:  step, i, j (counters) ↤ 0
7:  Ω_c ↤ 0
8:  for step < iterations do
9:          for i < grid-length(Ω_c) do
10:                 for j < grid- length(Ω_c) do
11:                         if c(i,j) > 0 then
12:                                 Ω_c(i,j) = 1
13:                         end if
14:                 end for
15:         end for
16:         for i < grid do
17:                 for j < grid do
18:                         if Ω_c(i,j) == 1 then
19:                                 u_new(i,j) = u_old(i,j)+∇²(u_old(i,j))+substrate·ζ(κu_old(i,j)+u_old(i,j)²-λu_old(i,j)v_old(i,j))
20:                         end if
21:                         v_new(i,j) = v_old(i,j) + d∇²(v_old(i,j)) + ζ (μu_old(i,j)³- v_old(i,j))
22:                         if u_new(i,j) ≥ threshold then
23:                                 a(u_new(i,j)) = ξ
24:                         else
25:                                 a(u_new(i,j)) = ξ - ϑ(u_old(i,j) - threshold)
26:                         end if
27:                         c_new(i,j) = c_old(i,j) + Ω_c ζ v c_old(i,j)(a(u) - c_old(i,j))(c_old - 1)
28:                 end for
29:         end for
30:         if u_new(i,j) > a_max then
31:                 u_new(i,j) = a_max
32:         end if
33:         if v_new(i,j) > i_max then
34:                 v_new(i,j) = i_max
35:         end if
36: end for
```

In conclusion, the model's growth is succinctly described by a three-way interaction, in which the space Ω_C permits values for the activator, which subsequently stimulates the growth of the mycelium.

The FUNGATERIA project has received funding from the European Union's HORIZON-EIC-2021-PATHFINDER CHALLENGES programme under grant agreement No. 101071145

Co-funded by the European Union

European Innovation Council

Following this, Ω_C is updated and expands in regions where c is non-zero. This process is repeated and establishes the use of the variable range Ω_C.

2.2 Simulation results

The results of the 2D model's simulations are presented in this paragraph, proving that it can accurately replicate fundamental mycelium behaviors like tip extension, branching, and anastomosis, confirming its ability to mimic fungal-based ELMs. By simulating these processes, the model looks like a fungus, especially by reflecting the patterns found in fungi, especially those in the Rhizoctonia Solani family [42]. This lends credibility to the modeling results. It is noteworthy that the employed model is not used to represent specific chemical species. Instead, it serves as a mathematical framework designed to broadly and effectively capture the dynamics of the system, aiming to accurately simulate the evolution of mycelium. The involved abstract variables are employed to model the emergent patterns and behaviors seen in the ELM bio-inspired system, rather than directly representing particular chemical entities. In addition, simulation results for the 3D model, an extension of the 2D model, are presented. Finally, it should be noted that the values of the utilized parameters are seen in Table I.

Table I. Utilized Evolution Parameters

Paremeter	Value	Paremeter	Value
$\boldsymbol{\theta}$	2.5	$\boldsymbol{\nu}$	1
$\boldsymbol{\zeta}$	625	$\boldsymbol{\xi}$	0.49
$\boldsymbol{\kappa}$	0.5	$\boldsymbol{a_{max}}$	20
$\boldsymbol{\lambda}$	0.8	$\boldsymbol{i_{max}}$	30
$\boldsymbol{\mu}$	2.6	$\boldsymbol{threshold}$	0.5
$\boldsymbol{d}$	30	$\boldsymbol{\rho}$	0.7

2.2.1 2D model results

In Fig. 4, the CA-based mycelium's growth is depicted, which is shown at different simulation steps. One can observe the condensed biomass at the center, while the hyphae are visible at the periphery. This is accomplished by alternating between the two kernels, ∇_A^2 and ∇_B^2, in a 3:1 ratio, respectively, every 100 iterations, following in a sense the natural process. This means that, every 100 iterations, diffusion is performed with ∇_A^2 for 75 iterations and with ∇_B^2 for the remaining 25 iterations.

Focusing on Fig. 5, the patterns of the activator, suppressor, and mycelium are very similar. This is reasonable given that the activator's growth, which the suppressor shapes, directly affects the mycelium's state. Furthermore, their concentration ranges are represented on the corresponding color bars. Additionally, in areas where the substrate is more prosperous (closer to 1), there is a higher concentration of the activator, which results in a thicker cell structure. The model also randomly introduces obstacles, for example rocks, within the substrate, which impede the growth of the ELM in those specific areas.

The FUNGATERIA project has received funding from the European Union's HORIZON-EIC-2021-PATHFINDER CHALLENGES programme under grant agreement No. 101071145

Co-funded by the European Union

European Innovation Council

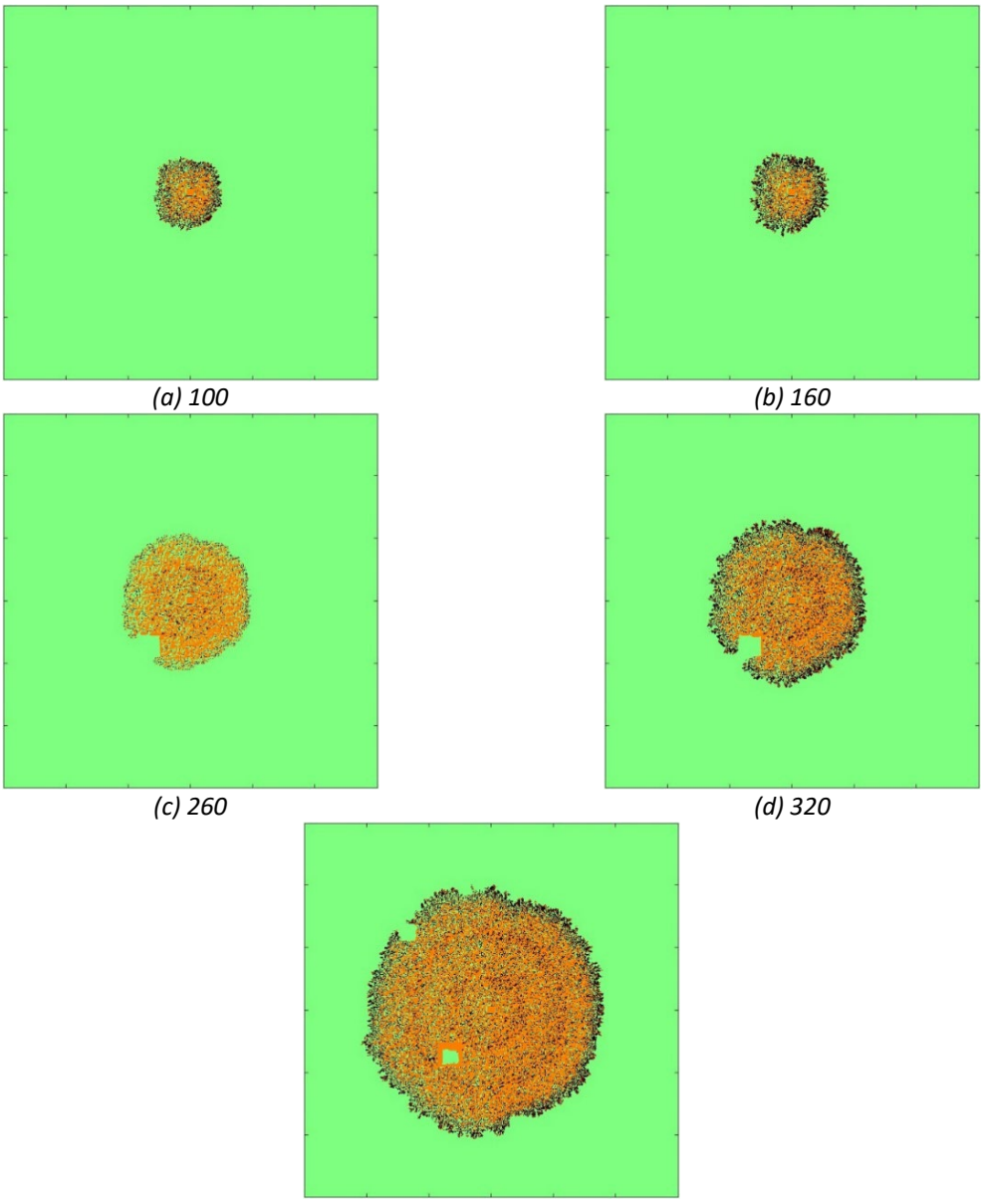

(a) 100 *(b) 160*

(c) 260 *(d) 320*

(e) 480

Fig. 4. Mycelium concentration c at different simulation steps for the 2D model

Moreover, the fundamental mycelium-based ELM mechanisms which include hyphae extension, apical and lateral branching, anastomosis and nutrient uptake are observed and showcased in Fig. 6, which is a magnification of the mycelium's state in Fig. 4(c). Extension, branching, and anastomosis are readily observable in the mycelium's hyphae, while nutrient uptake is indicated by the density of the activator. The substrate morphology results in a denser right region, as shown in Fig. 6(d).

The FUNGATERIA project has received funding from the European Union's HORIZON-EIC-2021-PATHFINDER CHALLENGES programme under grant agreement No. 101071145

Co-funded by the European Union

European Innovation Council

Fungateria

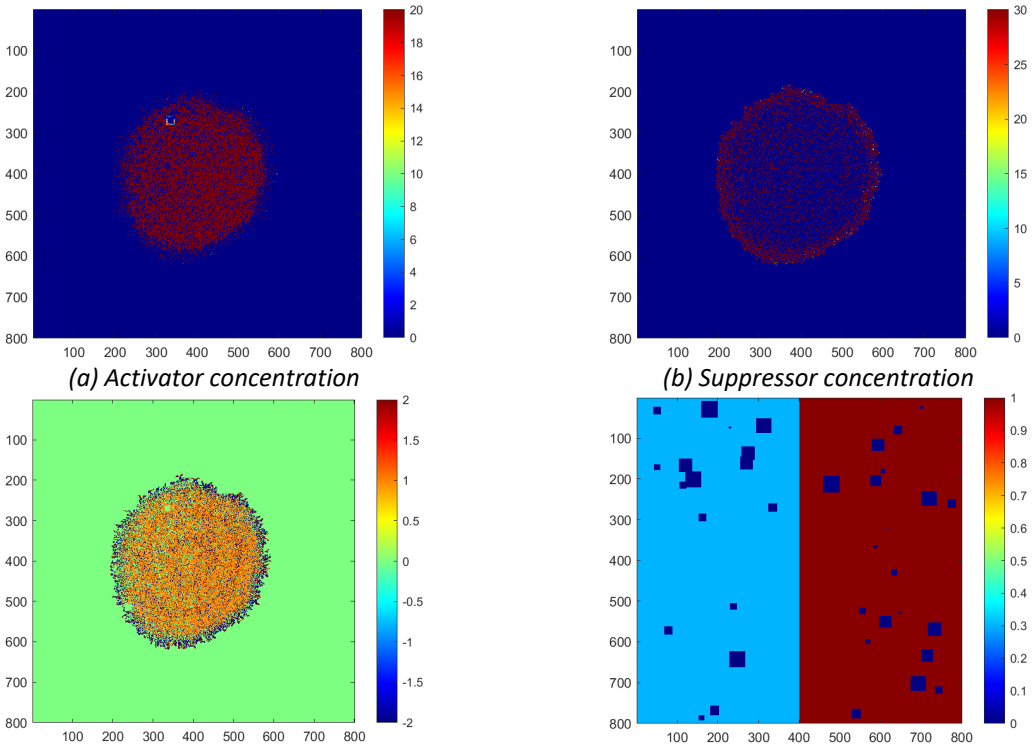

(a) Activator concentration

(b) Suppressor concentration

(c) Mycelium State

(d) Substrate

Fig. 5. (a-c) Final patterns of the activator, suppressor concentration and mycelium state respectively after 500 timesteps, and (d) substrate initialization for the 2D model

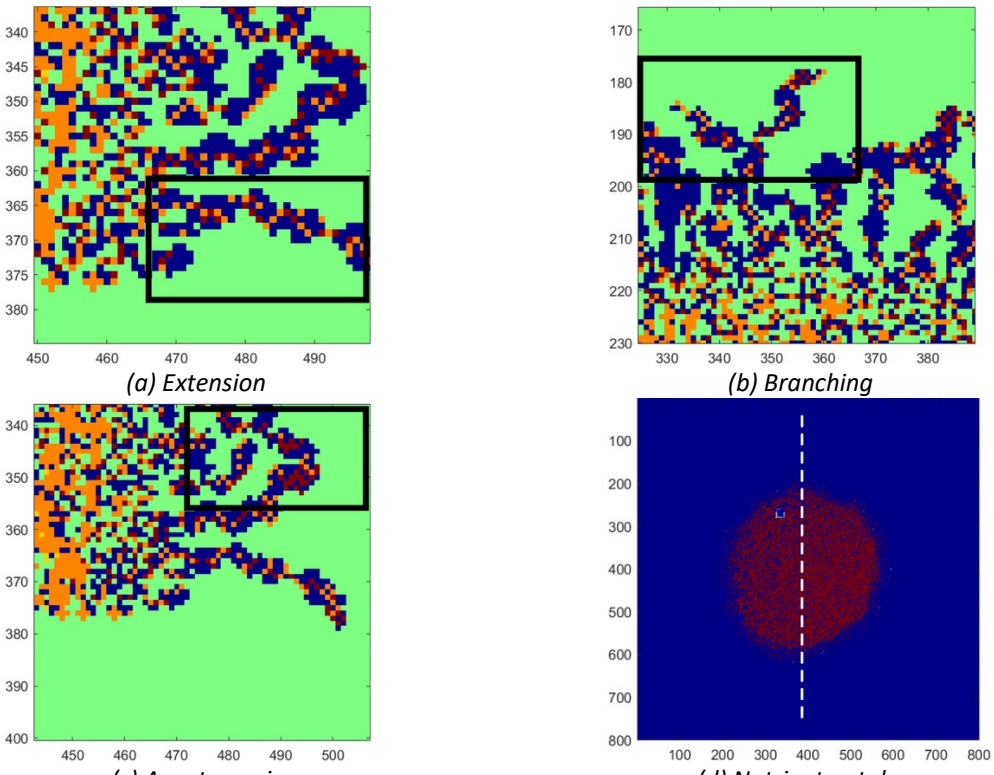

(a) Extension

(b) Branching

(c) Anastomosis

(d) Nutrient uptake

Fig. 6. (a-c) Simulated biological mechanisms of the mycelium's hyphae depicted in the mycelium's concentration c, and (d) nutrient uptake and mycelium's density depicted in the activator's concentration u

The FUNGATERIA project has received funding from the European Union's HORIZON-EIC-2021-PATHFINDER CHALLENGES programme under grant agreement No. 101071145

Co-funded by the European Union

European Innovation Council

Fungateria

2.2.2 3D model results

In Fig. 7, the results of the 3D model simulation are presented. The augmentations consistently maintain the integrity of the 2D model's design, effectively showcasing the condensed biomass along with the precise spherical morphology of the fungi. These enhancements support the spatial and structural fidelity of the model and underline the robustness of the simulation parameters in replicating complex biological forms. Detailed visualization aids in understanding the dynamic interactions and growth patterns within the modeled environment.

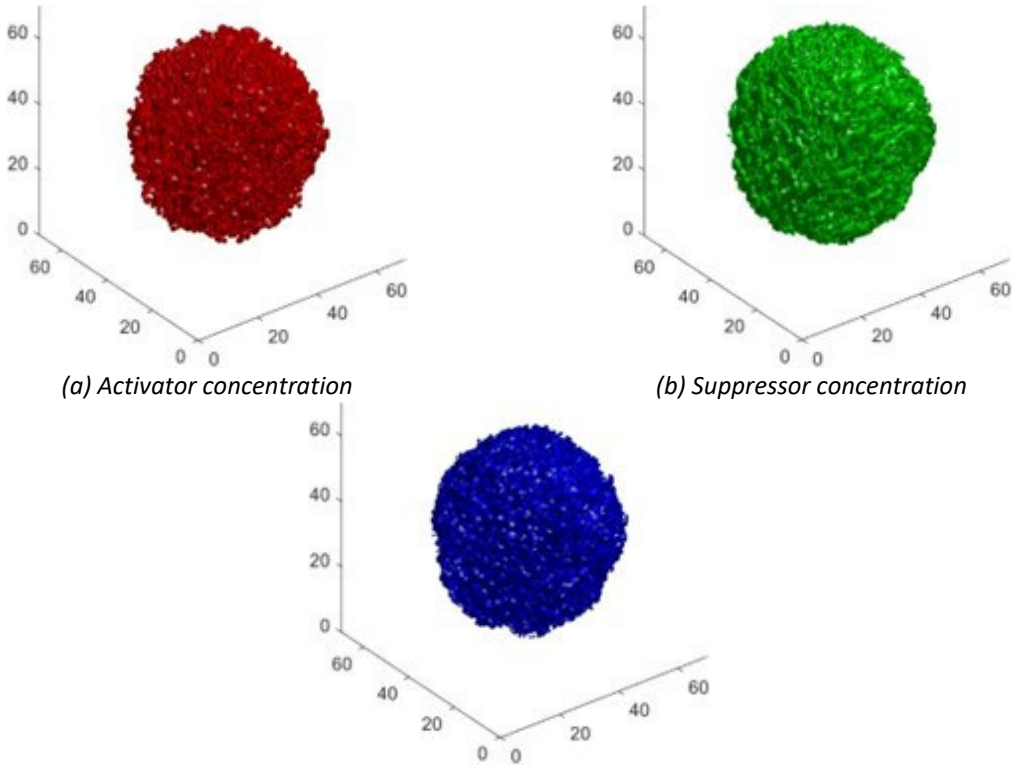

(a) Activator concentration

(b) Suppressor concentration

(c) Mycelium state

Fig. 7. Final patterns of the activator, suppressor concentration and mycelium state respectively after 100 timesteps for the 3D model

The FUNGATERIA project has received funding from the European Union's HORIZON-EIC-2021-PATHFINDER CHALLENGES programme under grant agreement No. 101071145

Co-funded by the European Union

European Innovation Council

Fungateria

3 Hardware implementation of DTP with FPGA

FPGAs excel in handling parallel computations due to their array of configurable logic blocks that can be programmed to perform discrete operations simultaneously. Field-Programmable Gate Arrays (FPGAs) are highly compatible with the implementation of Cellular Automata (CAs) due to their ability to perform parallel computations, aligning perfectly with the CA's simple, local, and parallel processing characteristics. This synergy facilitates the development of real-time, dynamic emulation crucial for modeling complex systems such as Engineered Living Materials (ELMs). Additionally, utilizing FPGAs could examine the establishment bidirectional communication with mycelium-based ELMs through integrated analog-to-digital converters (ADCs) and digital-to-analog converters (DACs). This setup could enable the translation of biological signals into digital data for comprehensive analysis but also allows for the real-time return of operational commands to the living materials. By utilizing the analog ports on the FPGA to connect with environmental sensors measuring variables like humidity, temperature, and soil quality, the digital twin could dynamically reflect and adapt to the conditions affecting the biological counterpart, ensuring a high-fidelity emulation and interaction between the digital and biological systems.

Algorithm 2. Mycelium-based ELM model utilized for the FPGA implementation (iterative process)

1: $N \leftrightarrow$ *evolution enable matrix*
2: $n \leftrightarrow$ *substrate nutrient matrix*
3: **if** codeselector == 1 **then** $L \leftrightarrow L_1$ **else** $L \leftrightarrow L_2$
4: $u_{new} = u_{old} + N \circ (conv(u_{old}, L)) + n\zeta(\kappa u_{old} + u^2_{old} - \lambda u_{old} v_{old})$
5: $v_{new} = v_{old} + d\ (conv(v_{old}, L)) + \zeta(\mu u^3_{old} - u_{old})$
6: $c_{new} = c_{old} + \zeta v c_{old}\ (a(u_{old}) - c_{old})\ (c_{old} - \rho)$
7: **if** $u_{old} \geq$ threshold **then** $a(u_{old}) = \xi$ **else** $a(u_{old}) = \xi - \vartheta(u_{old} - threshold)$
8: **if** $a(u_{old}) < 0$ **then** $c_{new} = 1$
9: **if** $u_{new} < 0$ **then** $u_{new} = 0$
10: **if** $u_{new} > a_{max}$ **then** $u_{new} = a_{max}$
11: **if** $v_{new} > i_{max}$ **then** $v_{new} = i_{max}$
12: $v_{old} = v_{new};\ u_{old} = u_{new};\ c_{old} = c_{new};$

3.1 System design and architecture

The CA's principles (state, rule, and neighborhood) are fully compatible with digital hardware implementations, as they can be effectively represented using memories and logic. These memory units function as matrices which can be modified at each timestep, dictated by the programmed logic. This setup facilitates easy reading from/writing to the memory (state and rule), and efficiently manages local interactions (neighborhood) within each cell of the CA. Moreover, this method is not only highly compatible with existing hardware, but also enhances computational efficiency through significant parallelism [43], where all calculations occur within a narrowly defined time window, specifically the simulation's time step, set by the clock. As a result, the FPGA is a very promising digital platform to implement CAs, incorporating the hardware to effectively support all the above requirements. The

The FUNGATERIA project has received funding from the European Union's HORIZON-EIC-2021-PATHFINDER CHALLENGES programme under grant agreement No. 101071145

Co-funded by the European Union

European Innovation Council

Fungateria

proposed CA was implemented using High-Level-Synthesis (HLS) [44] using the AMD Vitis Software and the Xilinx ZedBoard Zynq 7000 ZC702 Evaluation Board (xc7z020clg484-1).

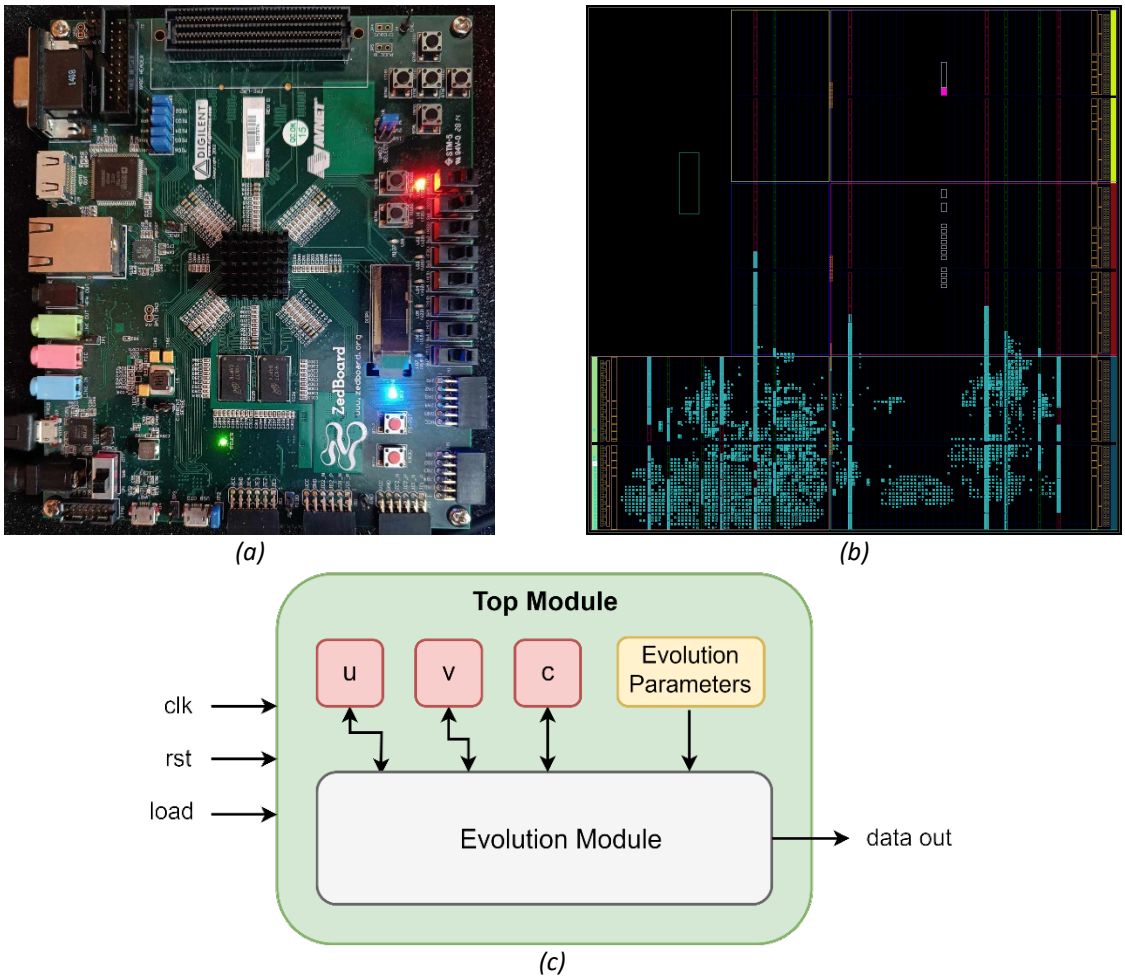

Fig. 8. (a) Snapshot of the utilized FPGA, (b) occupancy of the hardware resources of the device after the implementation step, and (c) qualitative block diagram of the design in the FPGA

The algorithm used for the HLS, written in C++, is described in Algorithm 2. The model initiates a loop phase continuously updating at each iteration. Initially, the neighborhood matrix is established. Subsequent updates are governed by the code selector variable, a binary vector comprising sequences of $0s$ and $1s$, which determines when the rule update of the cellular automaton is altered. The first rule (lines 1-4) facilitates a more circular diffusion by employing a kernel with diminished weights on the diagonal, whereas the second rule utilizes a kernel with equal weights on adjacent and diagonal positions. Updates to the values of the activator u, suppressor v, and the main body c are conducted in accordance with equations (1)-(4) and the appropriate Laplacian kernels extracted that emerges from equation (5), namely L_1 and L_2 to represent the two different CA rules. The two kernels are seen as follows in equation (8):

$$L_1 = \begin{pmatrix} 1/10 & 7/20 & 1/10 \\ 7/20 & -1/9 & 7/20 \\ 1/10 & 7/20 & 1/10 \end{pmatrix}, \quad L_2 = \begin{pmatrix} 0 & 1/20 & 0 \\ 1/20 & -1/5 & 1/20 \\ 0 & 1/20 & 0 \end{pmatrix} \quad (8)$$

The FUNGATERIA project has received funding from the European Union's HORIZON-EIC-2021-PATHFINDER CHALLENGES programme under grant agreement No. 101071145

Co-funded by the European Union

European Innovation Council

Fungateria

The neighborhood, replicating a circular front, is also multiplied with the diffusion term of the RD processes, to support the radial growth of the activator, adjacent to the main body. Limiters are then applied to both the activator and suppressor to prevent excessively large values that could impede the diffusion process. Finally, the states of the activator, suppressor, and main body are updated.

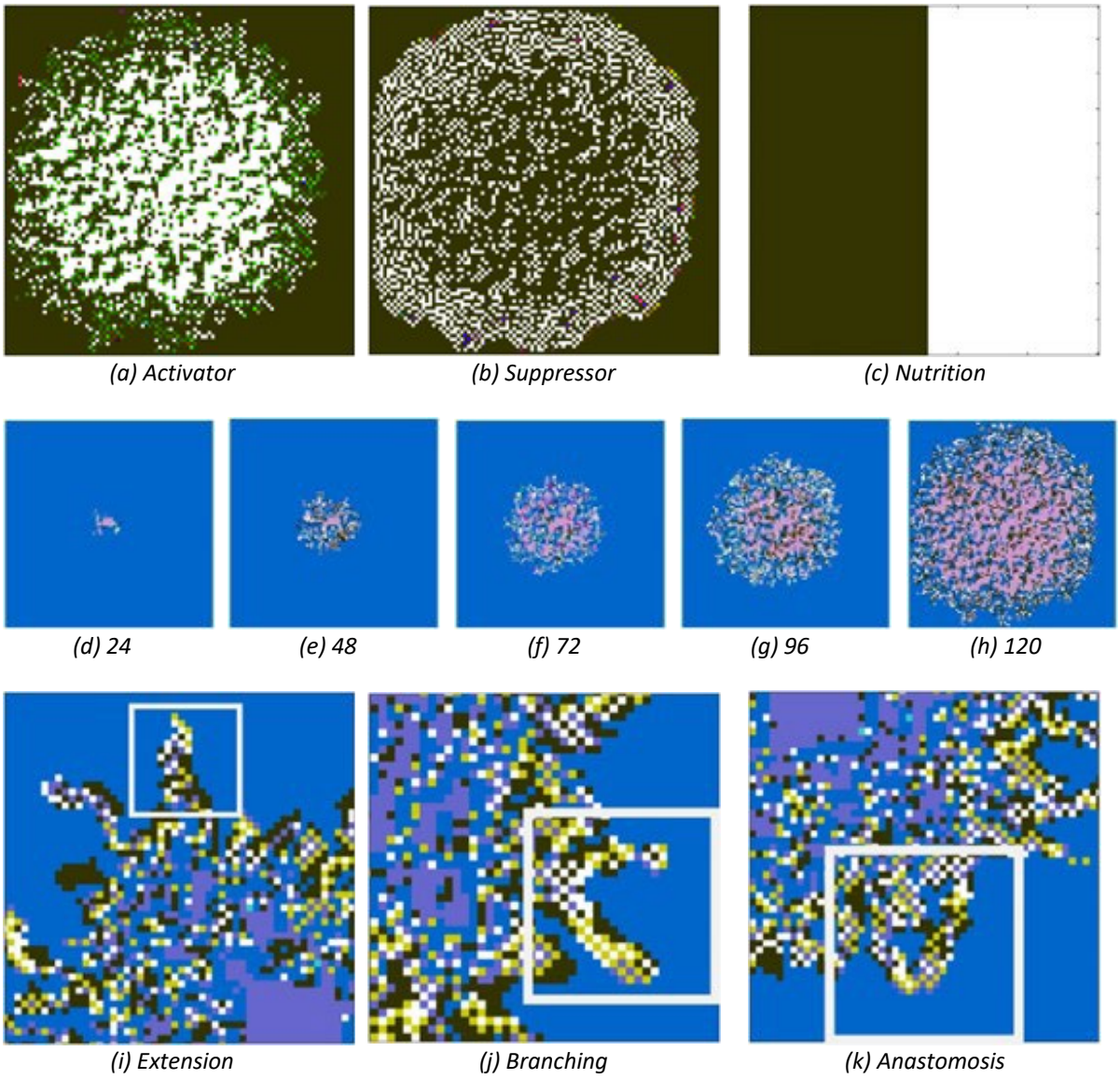

(a) Activator *(b) Suppressor* *(c) Nutrition*

(d) 24 *(e) 48* *(f) 72* *(g) 96* *(h) 120*

(i) Extension *(j) Branching* *(k) Anastomosis*

Fig. 9. (a) Activator u, (b) suppressor v, (c) nutrient concentrations across the grid at 120 simulation's iterations, (d)-(h) mycelium main body concentration c at different simulation's iterations, while in (a)-(h), the lighter color corresponds to higher concentration, and (i)-(k) mycelium's tip mechanisms, where simulations were conducted for 120 iterations at a 100x100 grid

The memory needed to uphold the state of the CA is divided into 3 two-dimensional matrices containing the activator, the suppressor, and the main body's values, which utilize the board's BRAM blocks. The rule principle of the CA is implemented in the FPGA, utilizing the board's look-up-tables (LUTs), which are reprogrammable combinational logic blocks containing logic gates capable of handling the complex RD processes. As seen in Fig. 8(a), the design comprises an evolution module, which is responsible for the computing of the next state of the mycelium's evolution and a top module.

The FUNGATERIA project has received funding from the European Union's HORIZON-EIC-2021-PATHFINDER CHALLENGES programme under grant agreement No. 101071145

Co-funded by the European Union

European Innovation Council

Fungateria

The evolution module takes as input the *evolution parameters* first initialized in the top module and returns the state of the evolution as *data out*, and the three state tables u, v, and c to it, to get renewed for the next iteration of the evolution. So, there is a feedback mechanism between the evolution module and the top module to take the previously computed state as an input to the next iteration.

3.2 Simulation results

In Figs. 9(d)-(h), the growth of the CA-based mycelium is depicted at various simulation steps, highlighting a dense biomass center marked by both mycelium cells and an activator, with hyphae visible on the stem. The suppressor's density increases toward the edges and decreases toward the center, illustrating its inverse relationship with both the activator and cell states. Figs. 9(a), (b), and (h) how the patterns of the activator, suppressor, and the mycelium's main body are closely aligned. Following, Fig. 9(c) displays the substrate that can affect the mycelium's ability to grow; more conducive areas (indicated by white/bright colors) promote a higher activator concentration and denser mycelium body.

It is important to note that in order to achieve the most accurate outcomes, a central zone was initialized with minimal concentrations of the activator, the suppressor, and the main body, representing the initial state of the mycelium, along with all the corresponding RD parameters. It is important to acknowledge that the initialization in the central area is conducted randomly. Considering the sensitivity of reaction-diffusion systems [41], this initial randomness is propagated across the evolving pattern with each iteration.

Table II. Utilization of the FPGA's resources after implementation

Resource	Utilization	Total Available	Utilization *(%)*
LUT	5,787	53,200	10.88
LUTRAM	308	17,400	1.77
FF	2,142	106,400	2.01
BRAM	66	140	47.14
DSP	63	220	28.64
IO	23	200	11.50
BUFG	5,787	53,200	10.88

Reaction-diffusion models featuring suppressors and activators offer a compelling framework for simulating the complex behaviors of mycelial growth, including tip extension, branching, and anastomosis, that are readily observable in the mycelium's hyphae. The validation of the result is based on the appearance of these three characteristics (extension, branching, and anastomosis) in every run of the simulation, as it is initialized with different u and v tables. It is noted that the proposed model is a generic reaction-diffusion model that is able, with the proper tuning of its parameters, to replicate the evolution of mycelial networks denoted by the three characteristics. As the activator promotes growth and propagation, the suppressor regulates and constrains this growth. Tip extension is naturally simulated as the activator diffuses outward, driving the elongation of mycelial hyphae. Branching emerges when local variations in activator and suppressor concentrations lead to spatial gradients, prompting the formation of new growth points. Anastomosis, the fusion of hyphal strands can be effectively simulated through the interaction of activator fronts, where collisions inhibit further propagation. These mechanisms are observed and showcased in Figs. 9(i)-(k). These processes have been regulated due to mechanisms for nutrient uptake by the table n, that also indicates the density of the activator u.

The FUNGATERIA project has received funding from the European Union's HORIZON-EIC-2021-PATHFINDER CHALLENGES programme under grant agreement No. 101071145

Co-funded by the European Union

European Innovation Council

Fungateria

Other than that, the modeling scale involves discretizing space into square lattice sites, each with a side length of $100\ um$ [14], encompassing a simulated grid area of $1\ cm^2$. With a small tradeoff in accuracy and adjustment of parameters, even larger mycelium structures can be emulated on the same grid, offering flexibility in modeling various mycelial configurations.

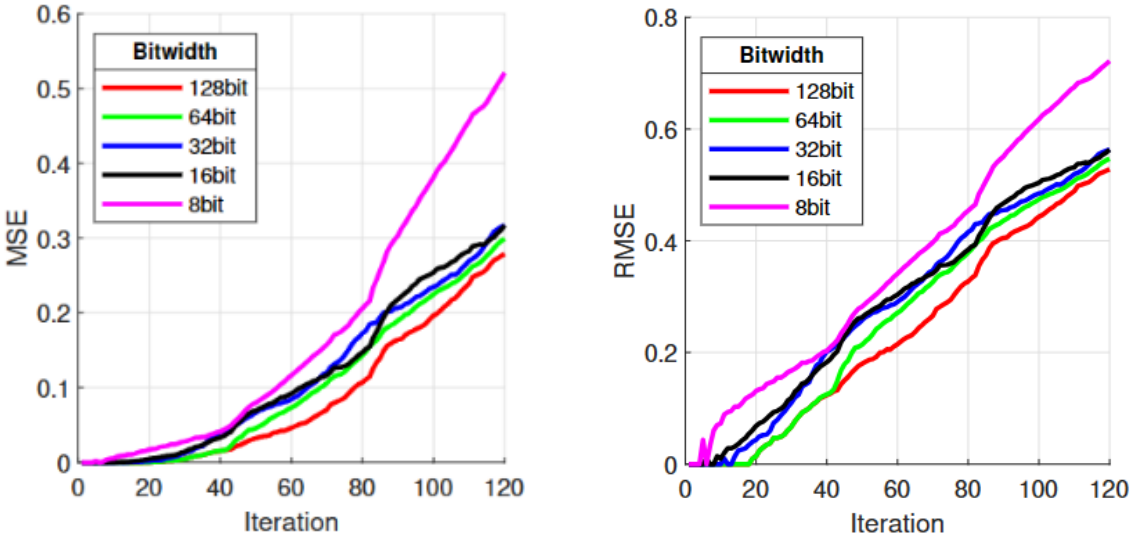

(a) (b)

Fig. 10. (a) Mean Squared Error (MSE) and (b) Root Mean Square Error (RMSE) observed during the iterations of mycelium's evolution between software and hardware simulation using different bitwidths

There have been various evolution implementations of the proposed design using different bitwidths for the computations. As one can notice, in Fig. 10, using 16 bits the evolution performs well with similar MSE and RMSE metrics compared to the higher bitwidth options, during the iterations. For 16-bit bitwidth, the hardware resources are seen in Table II, while in Fig. 8 (b) one can notice how the hardware resources are occupied on the board. It is noticed that it has been observed that using 32 bits, the accuracy of the evolution was almost the same as 16 bits, but the utilization of BRAMs and DSPs was doubled, as well as the consuming power. For this reason, the 16 bits bitwidth option is considered as the optimal for the proposed design.

Table III. Efficiency, execution time, and total energy metrics measured on CPU, GPU, and FPGA

Platform	Power *(Watts)*	Execution Time *(ms)*	Total Energy *(mJ)*
CPU	43.1	40	1,724
GPU	84.5	4.2	354.9
FPGA	0.37	35.1	12.9

Other than that, the algorithm has been implemented and tested in a CPU (Intel i9 9900k) and in a GPU (GeForce RTX 2060 Super), as observed in Table III. However, FPGA's parallelization capabilities along with its low power consumption makes it the most efficient candidate. To elaborate more, for the same computation load, FPGA appears to have the lowest energy need between CPU and GPU implementations, while utilizing the smaller area footprint as well. It is noted that the clock of the board is set to $10\ ns$, providing a running frequency of $100\ MHz$.

The FUNGATERIA project has received funding from the European Union's HORIZON-EIC-2021-PATHFINDER CHALLENGES programme under grant agreement No. 101071145

Co-funded by the European Union

European Innovation Council

Fungateria

4 Towards implementation of DTP with memristive circuits

Memristors, with their unique ability to both process and store information in a single component, are highly suitable for use in digital twins, particularly in the context of modeling Engineered Living Materials (ELMs). This suitability stems from their capacity to mimic the adaptive and evolutionary characteristics of biological systems. In the FPGA prototype of an ELM digital twin, specific analog hardware, including memristors, can be designed to emulate the electrical and morphological activities of ELMs. Memristors offer non-volatile memory, enabling them to maintain a state even when power is off, which mirrors the persistent nature of biological processes. Additionally, their ability to function at a low power consumption level, high density and their in-memory capabilities make them ideal for continuously running systems like digital twins, which require consistent data processing and updating. For this purpose, the emphasis is placed on using memristive nanoelectronic circuits to simulate biological mycelium's hyphae evolution and electrical activity.

4.1 Memristive Oscillating Cellular Automata for ELMs emulation

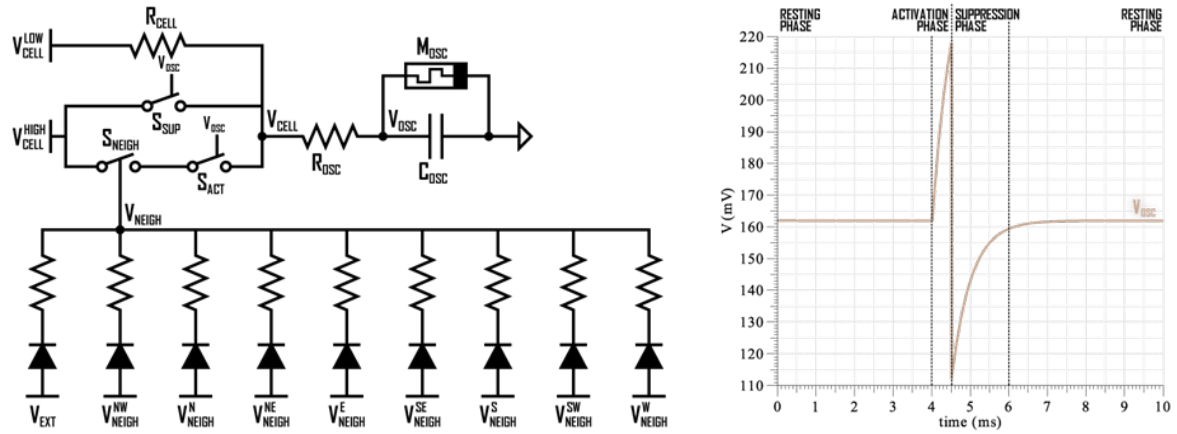

(a) *(b)*

Fig. 11. (a) Memristive Oscillating Cellular Automaton (MOCA) circuit, and (b) MOCA output oscillation and operational phases

To incorporate the necessary biological processes and mechanisms of mycelium-based ELMs, CAs are considered a good candidate as already discussed due to their denomination as an effective computational tool for simulating physical phenomena, leveraging their inherent parallel processing capabilities to perform computations efficiently when implemented in hardware [45]. Recent advancements in unconventional nanoelectronic devices, particularly memristors, have fueled the development of novel CA-based computing approaches. These include Memristive Cellular Automata (MemCA) [46] and Memristive Cellular Nonlinear Networks (M-CNN) [47]. A recent development introduces the Wave Cellular Automata concept, incorporating wave generation circuitry to mimic wave propagation within a cellular-like architecture [20]. These wave generators interconnect to form

The FUNGATERIA project has received funding from the European Union's HORIZON-EIC-2021-PATHFINDER CHALLENGES programme under grant agreement No. 101071145

Co-funded by the European Union

European Innovation Council

Fungateria

a network, enabling the propagation of electrical wave signals with the ability to interact spatially, replicating the core concepts of CA neighborhoods and evolution.

Following these principles and to integrate in circuit level the reaction-diffusion dynamics in a simplified manner, a Memristive Oscillating Cellular Automata (MOCA) configuration, illustrated in Fig. 11(a), is considered featuring an output voltage (V_{OSC}) oscillation mechanism (Fig. 11(b)) that fluctuates within specified voltage thresholds set by a unipolar memristive CBRAM device (M_{OSC}). This oscillation is achieved by connecting the cell to the voltage outputs of its immediate Moore neighborhood ($V_{NEIGH}^{NW;N;NE;E;SE;S;SW;W}$). An external voltage supply (V_{EXT}), which corresponds to external stimuli that affects hyphae evolution such as humidity, nutrients, light, etc., in parallel with the neighboring voltages allows the definition of distinct MOCA rules by properly affecting the connecting node (V_{NEIGH}). Different values to V_{EXT} leads to different values to V_{NEIGH}, which means that the threshold of the switch S_{NEIGH} can be reached easier or harder enabling different behaviors for each cell.

Oscillation initiation is triggered by applying a constant DC voltage, with the persistence of oscillations over time necessitating proper configuration of resistor (R_{OSC}) and capacitor (C_{OSC}) values. This prevents the voltage across the memristor (V_{OSC}) from reaching equilibrium between the oscillation thresholds. The voltage supplies V_{CELL}^{HIGH} and V_{CELL}^{LOW} deliver the necessary power through a two-branch control circuit: one maintaining the cell at idle state and another activating oscillation upon the appropriate rule conditions. An oscillation is initiated upon reaching the threshold determined by the applied rule, facilitated by a switch (S_{NEIGH}). To ensure proper MOCA operation and prevent abrupt oscillation interruption, a self-restraint switch (S_{ACT}) is incorporated in series with S_{NEIGH}. Furthermore, smooth operation is facilitated by the S_{SUP} switch, which guards against sudden oscillation halts and guarantees successful MOCA suppression, preventing rule influence on the computation time-step.

The MOCA operation can be categorized into three phases, namely resting, activation and suppression (Fig. 11(b)). In the resting phase, the oscillating unit remains idle, waiting to be triggered. The activation phase is initiated when a stimulus surpasses the MOCA activation threshold, triggering oscillatory behavior matching the function of the activator in a reaction-diffusion system. Finally, the suppression phase follows, where the oscillation reaches its minimum voltage level before increasing and returning to its resting state, corresponding to the suppressor behavior of a reaction-diffusion system. By connecting these MOCA cells in a spatial grid, it could emulate the ELM behavior focusing on their growth and evolution.

4.2 Variability tolerance analysis

The purpose of this paragraph is to assess the stability and consistency of the outputs generated by the designed memristive digital twin. To achieve this, a variability tolerance analysis is conducted to confirm the robustness of the proposed circuit architecture. As the project progresses, an investigation into the variability of memristive devices will be undertaken to simulate the aging process of the ELMs. The early incorporation of this aspect is crucial for the holistic evaluation of the system's performance over time.

The FUNGATERIA project has received funding from the European Union's HORIZON-EIC-2021-PATHFINDER CHALLENGES programme under grant agreement No. 101071145

Co-funded by the European Union

European Innovation Council

Fungateria

4.2.1 Utilized device variability

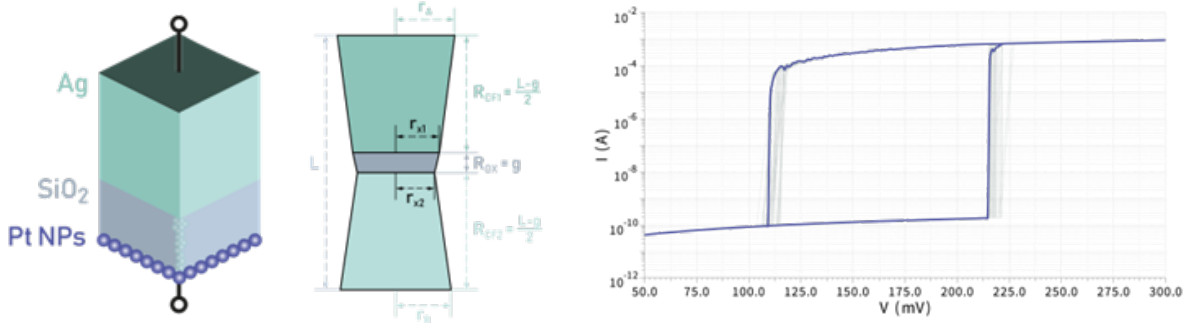

(a) (b) (c)

Fig. 12. (a) Structure of the fabricated CBRAM device. (b) Model representation for the CBRAM device. (c) I-V curves of the device utilized in the simulations. In solid lines the average curve is depicted, while faint lines indicate each distinct cycle employed

The utilization of memristors within MOCA cells is important in the generation of oscillations, which are indispensable for establishing a predefined time-step. In this work, Conductive Bridging RAM (CBRAM) modeled devices were employed due to their suitability for this application. To elaborate further, our oscillator requires a unipolar device to produce the necessary oscillations, while also taking into consideration physical parameters such as the temperature and the energy efficiency of the oscillating system. These devices base their operation in the electrochemical metallization principle, where a conductive metallic filament is formed during a SET operation, while the same filament undergoes a dissolution during a RESET operation in a solid dielectric material, referred as switching layer [48]. To achieve a realistic and seamless integration of these memristor devices within the simulated circuit, a compact memristor model as proposed by Fyrigos et al. [49] has been employed. This model adeptly encapsulates the intricate dynamics of unipolar CBRAM devices, incorporating essential attributes such as drift, diffusion, and thermo-diffusion effects, which are indispensable for simulating the switching behavior of memristors. In this way, the model can accurately capture the resistive switching operations of the used CBRAM devices, i.e. the formation and breakage of the Conductive Bridge (CB) between the active and inert electrodes (Fig. 12(b)). Notably, this model has been fitted to fabricated CBRAM devices of Ag/SiO_2/Pt NPs configuration (as seen in Fig. 12(a)) that exhibit unipolar characteristics.

Variability plays a pivotal role in the performance of electronic circuits and systems, a principle that extends to memristors as well [50]. The relentless trend towards the miniaturization of electronic components, while exacerbating the influence of variability on the performance and reliability of integrated circuits, has concurrently introduced additional, albeit less dominant, sources of random voltage and current fluctuations. These variations range from fluctuations in Random Telegraph Noise (RTN) currents to quantum mechanical-induced effects, such as direct tunneling and hopping effects [51]. Moreover, they encompass the more typical variations originating from manufacturing processes, resulting in device inhomogeneity, and the influence of environmental conditions, such as humidity and pressure, which can induce substantial deviations from the anticipated behavior of both individual devices and complete systems [52]. Out of these various sources of variability, they can be distinguished into two fundamental types: device-to-device (DTD) variability and cycle-to-cycle (CTC) variability [53]. CTC and DTD variability poses a critical challenge in ensuring the robustness and

The FUNGATERIA project has received funding from the European Union's HORIZON-EIC-2021-PATHFINDER CHALLENGES programme under grant agreement No. 101071145

Co-funded by the European Union

European Innovation Council

Fungateria

reliability of electronic systems [54], particularly in data sensitive applications, where even small deviations can lead to substantial errors and data degradation.

In the context of this study, we investigate the inherent variability in the behavior of the utilized CBRAM devices and its impact on the overall circuit performance. The I-V characteristic curves of the employed unipolar device during simulations are depicted in Fig. 12(c), where the solid line indicates the average I-V behavior over 200 periods and the faint lines indicate the respective behavior at each of these cycles. It becomes evident that the SET process is being triggered around 220mV , while for the RESET process ≃ 110mV are sufficient, with the device variability altering these values by ±1.5% and ±2.6%, respectively. This result demonstrates the stochastic nature of the CB formation and dissolution processes due to the combination of drift, diffusion, and thermo-diffusion effects. As the memristor plays a vital role in MOCA operation by producing the required oscillation, its variability impact on output oscillation requires to be properly investigated.

4.2.2 Impact of variability on oscillations

Focusing on complex circuits and systems, the propagation of variability may generate cascading effects, amplifying the impact on the overall system performance. In IC design such undesirable fluctuations can lead to compromised functionality and reduced yield. It is vital to understand these changes to mitigate the adverse effects and manage the impact of variability [55], enabling the design of robust and reliable electronic systems that can tolerate and adapt to component fluctuations, ensuring consistent and predictable performance under varying operating conditions.

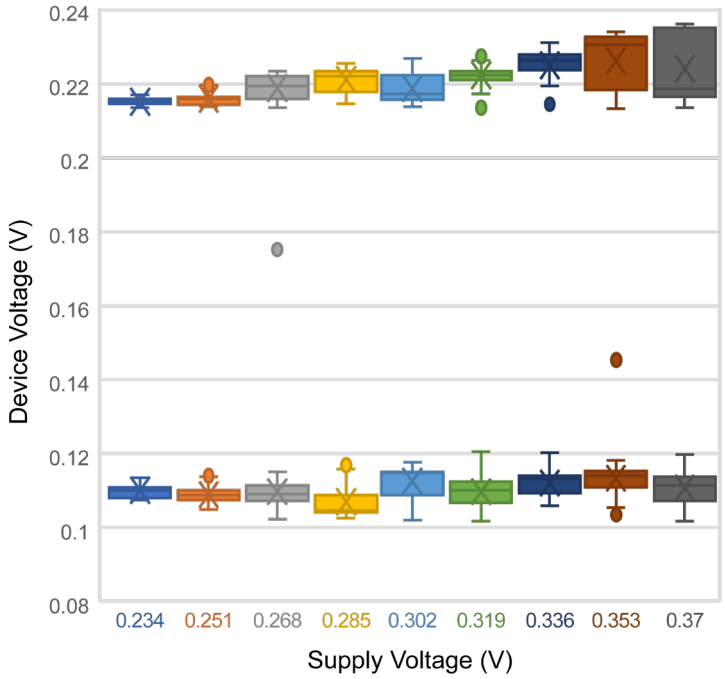

Fig. 13. Impact of variability in the range of lowest and highest voltage values under different V_{CELL}^{HIGH} supply voltages for the oscillating output (V_{OSC})

The FUNGATERIA project has received funding from the European Union's HORIZON-EIC-2021-PATHFINDER CHALLENGES programme under grant agreement No. 101071145

Co-funded by the European Union

European Innovation Council

Fungateria

Regarding the MOCA circuitry, and particularly the oscillatory part, the simulated distributions of the lowest and highest voltage variations seen in the output oscillation voltage amplitude V_{OSC} under different V_{CELL}^{HIGH} supply voltages are depicted in Fig. 13 for over 100 cycles. Thus, it becomes evident that the stochastic behavior of an oscillation is increasing by increasing the supply voltage to the oscillator unit. At the same time, there are cases (i.e. $0.268V$ and $0.353V$) where oscillation is falsely activated with catastrophic results for the computing outcome of the MOCA. Since oscillation synchronization is playing a vital role for the computing phase of the MOCA, it is important to keep variations as low as possible avoiding false activations. As such, the case of $V_{CELL}^{HIGH} = 0.251V$ is considered for a more detailed analysis.

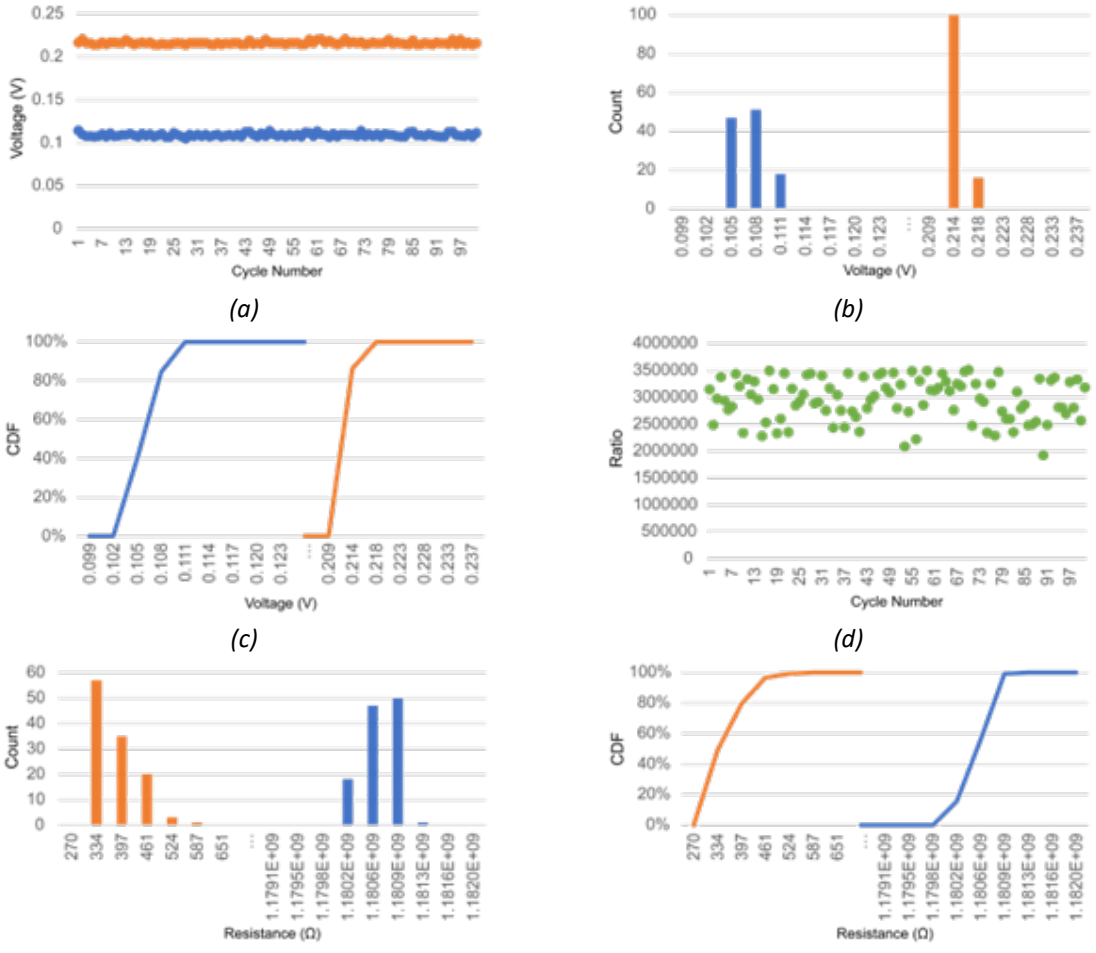

Fig. 14. (a) Evolution of the oscillation output V_{OSC} at the lowest and the highest oscillation voltages as a function of the number of cycles. (b) Distributions and (c) cumulative distribution functions of the oscillation output V_{OSC} at the lowest and the highest oscillation voltages. (d) SET and RESET resistances ratio as a function of the number of cycles. (e) Distributions and (f) cumulative distribution functions of the SET and RESET resistances. The simulations have been performed for $V_{CELL}^{HIGH} = 0.251V$.

In Fig. 14, key measurements regarding the impact of device's variability on the oscillation are presented, derived from a wide range of simulations. Beginning with Fig. 14(a), the time evolution of the oscillating output highest and lowest points is illustrated, denoted as V_{OSC}, across the entire span of simulation cycles. Subsequently, in Fig. 14(b), the histogram depicted represents the relationship between applied voltage amplitudes and the corresponding switching counts for both the SET and

The FUNGATERIA project has received funding from the European Union's HORIZON-EIC-2021-PATHFINDER CHALLENGES programme under grant agreement No. 101071145

Co-funded by the European Union

European Innovation Council

Fungateria

RESET operations that form a symmetric distribution. Fig. 14(c) showcases the cumulative distribution function (CDF) of the respective voltages with RESET voltages to showcase higher CTC variability effects. At this point, it is important to highlight that these oscillations points have presented a reduced variability effect to ±0.8% and ±1.8% for highest and lowest point accordingly. This can be attributed to the RC circuit in parallel with the CBRAM device that is able to minimize variability impact on oscillation through its time delaying and filtering phenomena.

Shifting our focus to Fig. 14(d), the High-Resistance State (HRS) to Low-Resistance State (LRS) switching ratio performance measured over successive cycles is presented showcasing a good state variability of the device to around 3×106 for most of the cases successfully serving the computing operations. In Fig. 14(e), the histogram displays the resistance values obtained in both HRS and LRS states, along with the frequency of their occurrence. It is evident that resistances in LRS present a positively skewed distribution, while in HRS a negatively skewed one, showcasing the resistance limits in which the oscillation changes slope. Finally, Fig. 14(f) presents the CDF corresponding to the information previously described.

All in all, the integration of variability-aware design methodologies can facilitate the optimization procedure of system-level performance metrics while accounting for the inherent variations in individual components. By incorporating statistical analysis, process variations can be effectively modeled and managed, enabling the development of robust circuit designs that are resilient to fluctuations in device parameters. Adopting a variability-aware design paradigm is crucial for addressing the challenges posed by component variability, enabling the development of next-generation electronic systems with enhanced performance, reliability, and efficiency. Our findings presented above indicate minor effect of variability in the operation of MOCA, which can be attributed to the proper design of the circuit which utilizes the RC effects in combination with unipolar CBRAM devices.

4.3 Simulation results on mycelium tip growth and branching

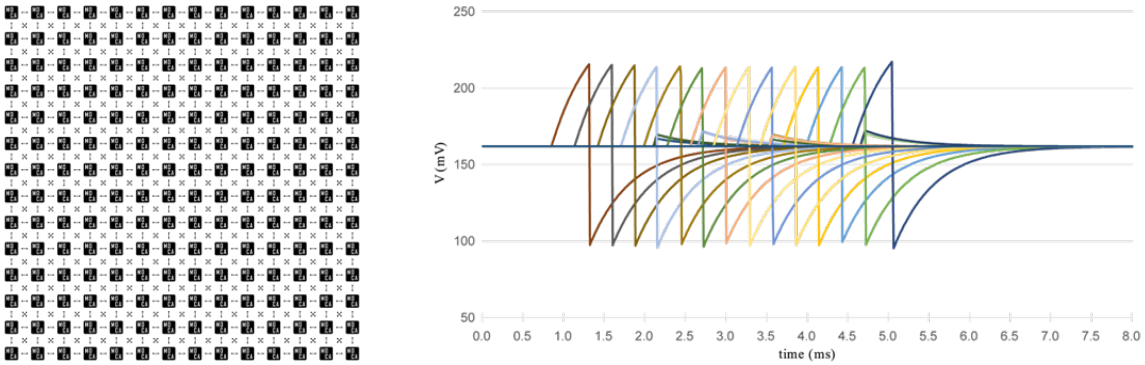

(a) *(b)*

Fig. 15. (a) A 14 × 14 grid of MOCA cells with their respective neighboring connections, and (b) output oscillations from all grid's MOCA cells

To simulate mycelium's hyphae propagation, a 14 × 14 grid of MOCA cells has been utilized as depicted in Fig. 15(a). All cells are connected through their Moore neighboring ones via their oscillation output V_{OSC} node. The voltage outputs of all cells are illustrated in Fig. 15(b) showcasing a domino effect of oscillation propagation in neighboring cells. In detail, when a cell is triggered, it enters its activation

The FUNGATERIA project has received funding from the European Union's HORIZON-EIC-2021-PATHFINDER CHALLENGES programme under grant agreement No. 101071145

Co-funded by the European Union

European Innovation Council

Fungateria

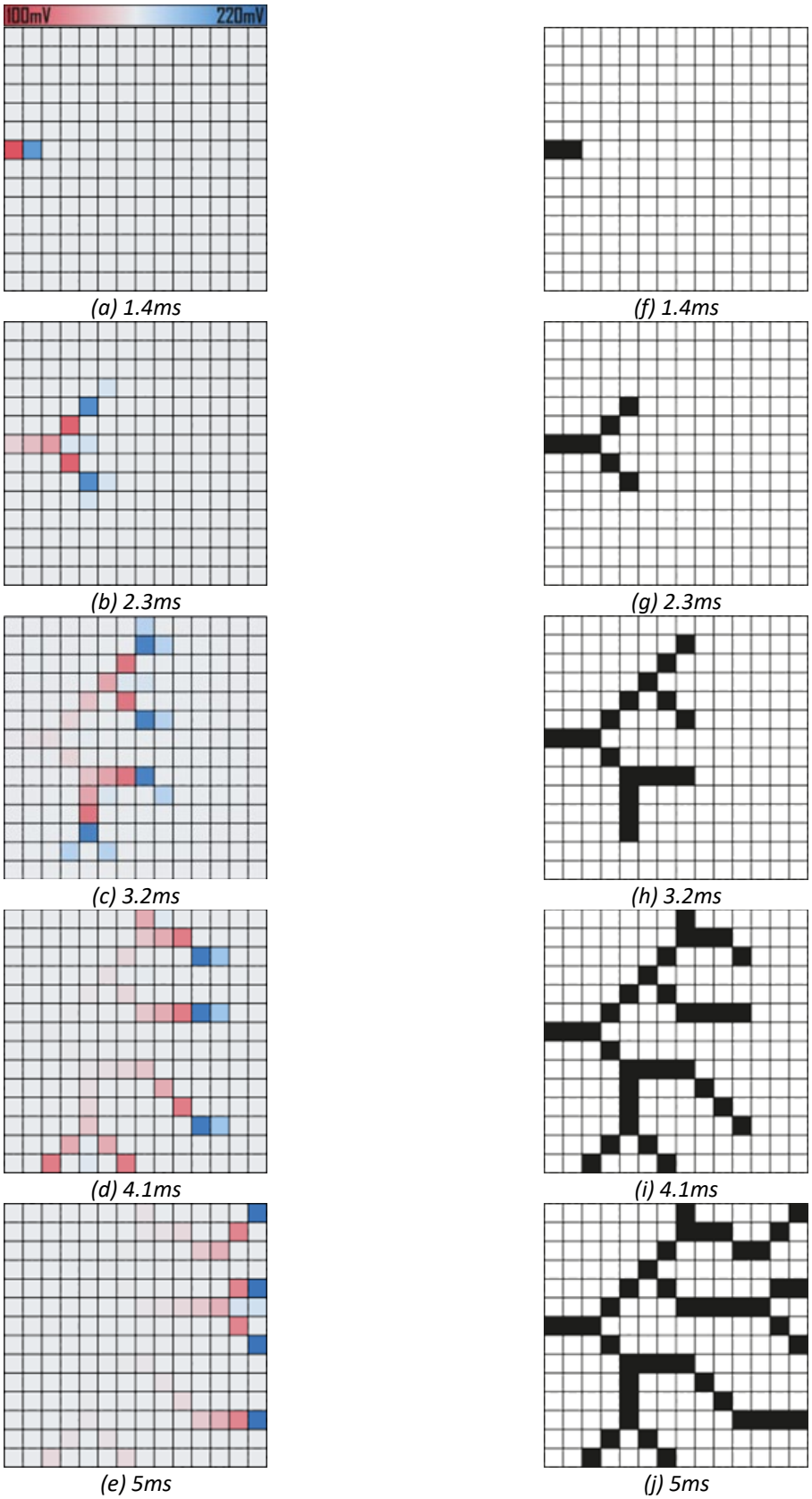

(a) 1.4ms (f) 1.4ms

(b) 2.3ms (g) 2.3ms

(c) 3.2ms (h) 3.2ms

(d) 4.1ms (i) 4.1ms

(e) 5ms (j) 5ms

Fig. 16. (a-e) Output voltages across the grid of MOCA cells in different simulation times. Blue corresponds to the activation phase, while red corresponds to the suppression phase. (f-j) Mycelium evolution after specific simulation times. Black cells correspond to the ones that have been already activated.

The FUNGATERIA project has received funding from the European Union's HORIZON-EIC-2021-PATHFINDER CHALLENGES programme under grant agreement No. 101071145

Co-funded by the European Union

European Innovation Council

Fungateria

phase and its output voltage increases. This affects its neighboring cells leading to the activation of some of them after some time. After the activation phase, the cell enters its suppression phase lowering its output voltage and leading to restraining its neighbor's activation. The impact of suppression phase can be clearly spotted at $2.2ms$, $3.6ms$ and $4.7ms$, where different cells attempt to initiate their activation, but the suppression effect of one of their neighbors restricts them and they return to resting phase.

To further clarify the triggering mechanisms within the cellular grid, snapshots of all cells output voltage are presented in Figs. 12(a-e) under different simulation times. The tip of the ELM is illustrated in deep blue when the cell is at the peak of its activation phase. The evolution begins from the left side of the grid (Fig. 16(a)) and the tip is growing progressively. In Fig. 16(b), the tip branching can be observed where two different tips are developed and propagated in the grid. The tip growth and branching continue in Fig. 16(c), while some of the branches are reaching the end of the grid in Fig. 5(d). It is important to highlight that suppressed cells are colored red restricting their neighbor's evolution like in the lower side of Fig. 16(d). The last activated cells can be observed in Fig. 16(e).

Following the operation of the MOCA grid, the evolution of the mycelium hyphae after specific times is illustrated in Figs. 12(f-j) with black color. The tip growth (Fig. 16(f)) and branching (Fig. 16(g)) are evident. In Fig. 16(h), the grid already includes 4 branches, while in Fig. 16(i) includes 5 of them proving that the evolution continues gradually. The complete evolution of the mycelium hyphae in the MOCA grid can be observed in Fig. 16(j), where the main mechanisms of growth and branching can be clearly spotted across the grid.

4.4 Electrical signal propagation in mycelium fungi with memristive circuits

4.4.1 Mapping mycelium grid in hardware

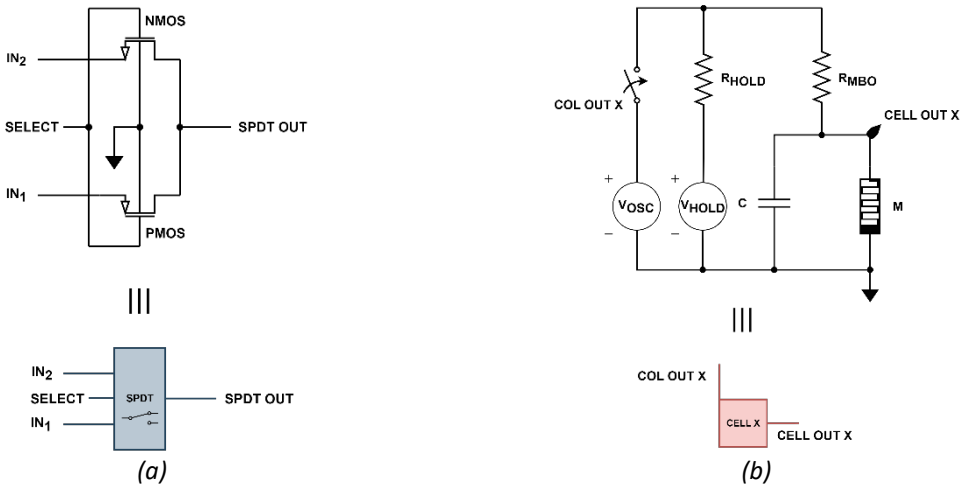

Fig. 17. (a) The SPDT circuit consisted by one NMOS and one PMOS transistor and its symbol, and (b) the circuit-level representation of a CA cell with its main component to be an MBO and its symbol

A mycelium evolution grid can be matched to CA cells grid which can change their state due to the Memristive-based Oscillator (MBO) they incorporate that is responsible for generating oscillations, depicting the electrical signal of mycelium fungi, each of which defines an evolution time step. In terms of cell's connecting neighbors, memristor also plays a critical role as it is mandatory for enabling the

The FUNGATERIA project has received funding from the European Union's HORIZON-EIC-2021-PATHFINDER CHALLENGES programme under grant agreement No. 101071145

Co-funded by the European Union

European Innovation Council

Fungateria

concept of training in the edges of the directed graph where the mycelium has been expanded. The equivalent circuit of a CA cell is spotted in Fig. 17(b), which contains a switch connected to its neighbors, two resistors R_{HOLD} and R_{MBO}, two voltage sources V_{HOLD} and V_{OSC}, a capacitor C and a memristor M forming a MBO able to generate neuron-like oscillations. Its function is characterized by two states, namely resting and computing. Finally, the cell's output is considered as the MBO output on the $CELL\ OUT\ X$ node.

Focusing on the functionality of the CA cell, this is continuously powered by the V_{HOLD} DC voltage to keep itself in the resting state taking advantage of the equilibrium point (EP), which is formed between the resistor R_{MBO} and the memristor M. More specifically, the EP can be observed on $CELL\ OUT\ X$, where its voltage is not sufficient to change the memristor state and the MBO cannot perform any oscillation. For the cell's rule to enable the oscillation, the necessary $COL\ OUT\ X$ voltage is provided on the respective switch and surpasses its threshold THR to trigger the second branch of the V_{OSC} DC voltage. This changes the voltage on the $CELL\ OUT\ X$ enabling the memristor state switch and the oscillation of the MBO. The resistor R_{HOLD} has been properly selected to switch between the two voltage sources with the least voltage deviations due to the Millman's theorem. Lastly, it is mentioned that the resistor R_{MBO} and the capacitor C affect the output oscillation form and timing.

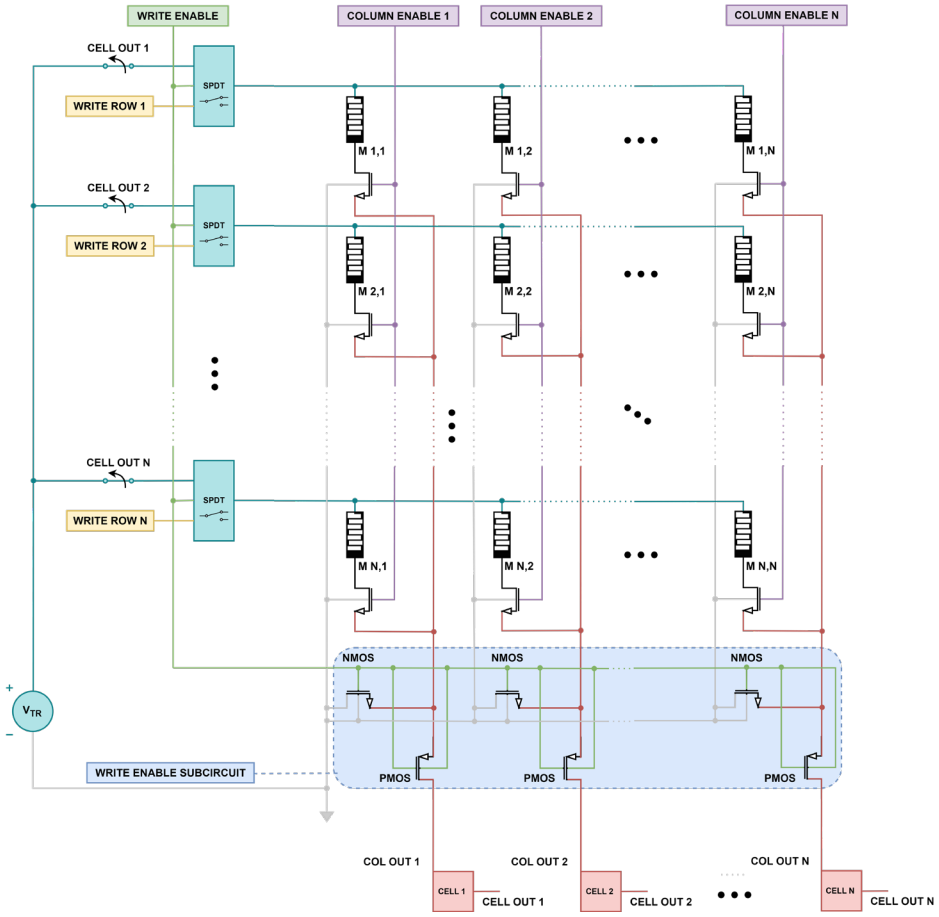

Fig. 18. The full designed circuit consisted of the crossbar, SPDT modules, the cells, and the required switches

After the design of the core part of the system, which is the CA cell, it should be incorporated into a circuit that encapsulates the mycelium evolution. The CA that is utilized is considered the N nodes of a mycelium graph, each of which represents a specific part of the mycelium grid. However, because

The FUNGATERIA project has received funding from the European Union's HORIZON-EIC-2021-PATHFINDER CHALLENGES programme under grant agreement No. 101071145

Co-funded by the European Union

European Innovation Council

Fungateria

the mycelium has been expanded only to part of the grid, the whole circuit consists of a crossbar with 1T1R components, the CA cells, a train-enable subcircuit, SPDTs, and regular switches as presented in Fig. 18.

Regarding CA's characteristics, the neighborhood of a cell includes all the other cells as the CA is a fully connected graph with trainable edges, i.e., neighboring connections. As for the cells' states, there are two as referred to in the previous paragrpah. In the resting state, the cell waits for the signal of the previous neighboring node so that can be triggered to the next state, computing. The latter corresponds to the increase of the voltage to produce an oscillation as Fig. 20 depicts. In this time domain simulation figure, colored areas represent the computing states of three (3) different CA cells. During this phase, the output signal passes through the crossbar and the next cell's computation is performed. After that, the next cell is triggered, and the cycle continues. The rule responsible for the activation of the cells is described by the following equation (9):

$$CELL_j = \begin{cases} computing\ state, & \sum_{i=1}^{N} \frac{SPDT\ OUT_i}{M_{i,j}} < THR \\ resting\ state, & otherwise \end{cases} \quad (9)$$

where N is the number of the CA cells (and of the total nodes as well), and i is the row and j the column number in the crossbar, accordingly.

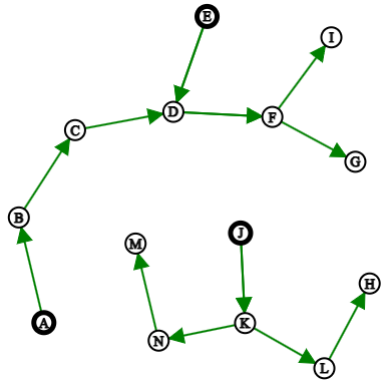

(a)

	A	B	C	D	E	F	G	H	I	J	K	L	M	N
A	0	1	0	0	0	0	0	0	0	0	0	0	0	0
B	0	0	1	0	0	0	0	0	0	0	0	0	0	0
C	0	0	0	1	0	0	0	0	0	0	0	0	0	0
D	0	0	0	0	0	1	0	0	0	0	0	0	0	0
E	0	0	0	1	0	0	0	0	0	0	0	0	0	0
F	0	0	0	0	0	0	1	0	1	0	0	0	0	0
G	0	0	0	0	0	0	0	0	0	0	0	0	0	0
H	0	0	0	0	0	0	0	0	0	0	0	0	0	0
I	0	0	0	0	0	0	0	0	0	0	0	0	0	0
J	0	0	0	0	0	0	0	0	0	0	1	0	0	0
K	0	0	0	0	0	0	0	0	0	0	0	1	0	1
L	0	0	0	0	0	0	0	1	0	0	0	0	0	0
M	0	0	0	0	0	0	0	0	0	0	0	0	0	0
N	0	0	0	0	0	0	0	0	0	0	0	0	1	0

(b)

Fig. 19. (a) The corresponding directed graph of the mycelium evolution, and (b) the respective Reference Matrix (RM) with "0" indicating the corresponding memristors to be written in OFF state (no edge between nodes), while with "1" to the ON state respectively (connecting edge between nodes)

The FUNGATERIA project has received funding from the European Union's HORIZON-EIC-2021-PATHFINDER CHALLENGES programme under grant agreement No. 101071145

Co-funded by the European Union

European Innovation Council

Fungateria

Concerning the crossbar configuration, its role is to store the edges of a specific train set of mycelium evolution to properly activate the respective cell in each timestep. It has been programmed during the training phase column-by-column using the ex-situ method with external binary weights as pulses of $0.5V$ amplitude and $4ms$ duration of a Reference Matrix (RM) presented in Fig. 19. This RM is externally trained utilizing the connections of Table III in such a way as representing the edges of the mycelium graph; so that the CA's evolution to be able to reveal a node sequence forming one or multiple branches. In this way the memristors of the crossbar can be written either in their ON or OFF state regarding the edge(s) that is (are) going to be formed. The graph utilized is a small one as proof of concept and for readability reasons, consisting of $N = 14\ cells$, so the RM have a size of 14×14. Each row represents the previous node, and each column has its following suitable node (s) for mycelium graph evolution that must train the edges of these nodes to produce the right sequence of electrical signal propagation. The rows of each branch's last node should be all filled by zeros as they do not trigger any other cell afterwards, while the columns of the branch's first node should be zeros as they are not previously connected to any other node. After the training phase, the circuit shall produce the corresponding branches(s) when triggering its (their) first cell.

The train-enable subcircuit (Fig. 18; light blue area) consists of two transistors, a NMOS and a PMOS and it has dual role. Firstly, it grounds the crossbar during the train phase, so that memristors to be written successfully as their bottom electrode will be in zero voltage. Secondly, it isolates the CA cells while the crossbar is being written to prevent their false activation. The module that allows the training is the SPDT switches. More specifically, they take the $WRITE\ ENABLE$ voltage as a select signal and they also have two different inputs, one used for writing the crossbar with ex-situ data (training phase), and the other for the evolution phase as presented in Fig. 17(a). To elaborate further, when the first input is activated, the memristors of the crossbar (which are also the connections of the CA cells) are trained following the RM topology. Otherwise, when the second input is activated, the evolution phase is enabled, and each row acquires a DC voltage V_{TR}. This voltage is subject to be dropped in specific rows to trigger the corresponding cells to their computing state and continuing the sentence forming. Every row is equipped with a normally closed switch behind the SPDT module that is responsible for generating the voltage drop that happens every time the cell corresponding to the previous node is in the computing state. Finally, it is worth mentioning that all the transistors used are modeled with the generic PTM model and appear gate length equal to $180nm$ technology node.

4.4.2 Simulation results

To simulate the corresponding circuit presented earlier, the Cadence Virtuoso Design Suite has been utilized. A set of 5 different branches is considered following derived mycelium evolution results from the previously described circuitry, and the expected output is presented to determine its proper functionality. As reported previously, the total number of cells used in the simulation is 14 and they appear in the RM of Fig. 19. The ideal electrical signal propagation sequences that the circuit should form are mentioned in Table III.

Table III. The set of branches being formed from the circuit

1:	$A \mapsto B \mapsto C \mapsto D$
2:	$E \mapsto D \mapsto F \mapsto G$
3:	$E \mapsto D \mapsto F \mapsto I$
4:	$J \mapsto K \mapsto L \mapsto H$
5:	$J \mapsto K \mapsto N \mapsto M$

The FUNGATERIA project has received funding from the European Union's HORIZON-EIC-2021-PATHFINDER CHALLENGES programme under grant agreement No. 101071145

Co-funded by the European Union

European Innovation Council

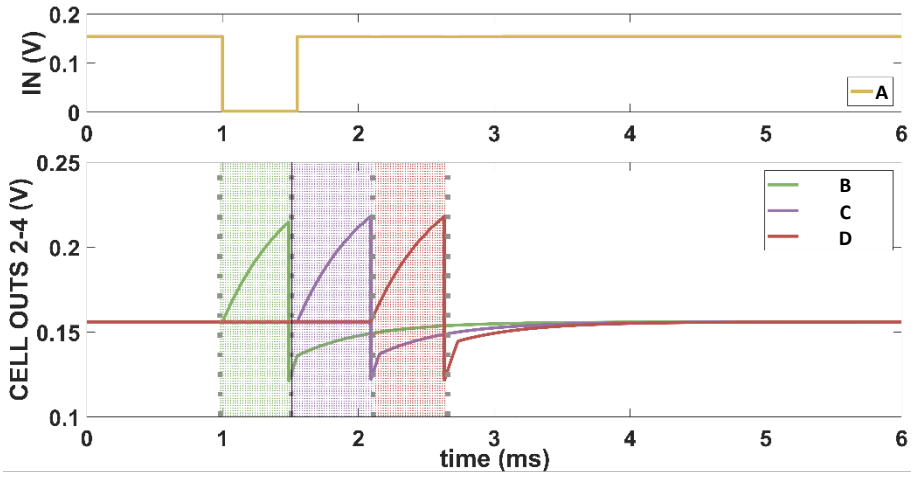

Fig. 20. Time domain simulations of the core CA circuits needed to form branch 1 of Table III; the activation of the corresponding cells happens after triggering the first node "A", while in each colored area the respective cell is in the computing state for one time step (0.55ms), and in white all are in the resting state

The branches can be separated into three distinct test cases deriving from their first node (i.e. "A", "E", and "J"). More specifically, in the first test case the circuit is requested to produce only the first branch in contrast to the second and third test cases that it is going to produce pairs of branches (2-3 and 4-5, accordingly). The scope of these test cases is to initially test the system in a simple task and then to more complex ones as it can be able to generate possible electrical signal propagation in different branches at the same time. The difference between the two (2) more difficult test cases is that the initial common nodes in the branches are reduced from three to two making the electrical signal propagation more complex and more difficult as more possible nodes should be triggered.

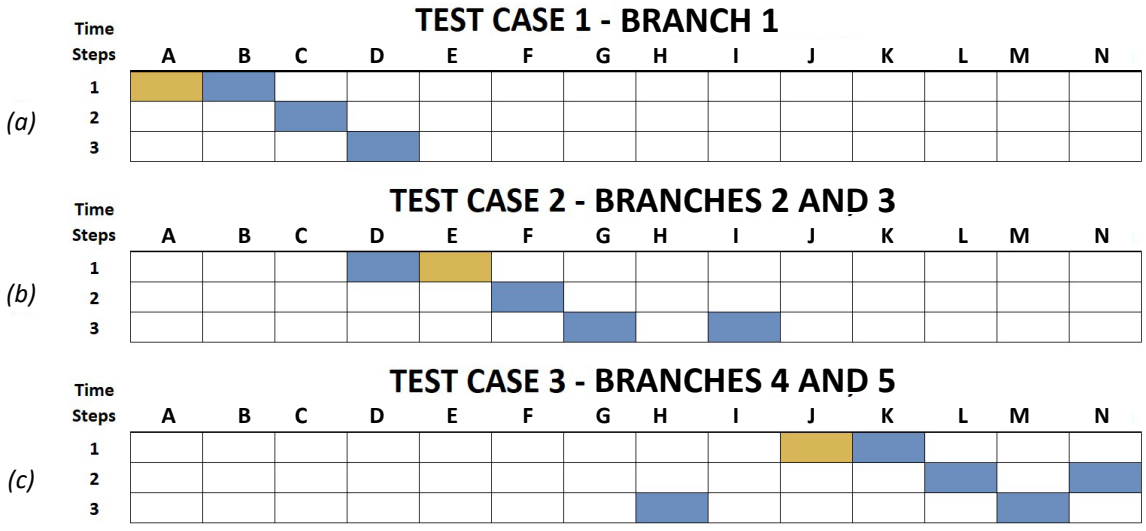

Fig. 21. Time domain evolution of the whole CA in steps (0.55ms each) forming the branches presented in Table III for three test cases, each of which is presented separately; in (a) branch 1 is being formed, in (b) branches 2 and 3 are being formed, and in (c) branches 4 and 5 are being formed

The electrical signal propagation in the branches is time dependent and is based on the cell's function as it has been described previously. First, in Fig. 20 the evolution of the first branch is presented. Here, in the beginning of the simulation the node "A" is externally triggered, and the CA is activating the

The FUNGATERIA project has received funding from the European Union's HORIZON-EIC-2021-PATHFINDER CHALLENGES programme under grant agreement No. 101071145

Co-funded by the European Union

European Innovation Council

proper nodes regarding the RM of the crossbar, in specific started with the node “B”, continued with “C”, and concluded with “D” successfully propagating the electrical signal in branch 1. All the other cells of the CA are resting. Note that the computing state of each cell lasts equal time ($0.55ms$) promoting the discrete time that characterizes a CA.

Following the previous example, a more holistic approach based on time domain simulation results is presented showing the evolution of the CA to the test cases that have been simulated. To elaborate, in Fig. 21, in the vertical axis, the time steps of evolution are depicted (each time step lasts for $0.55ms$) and in horizontal axis the 14 cells of the grid are depicted. With white is the initial state of the cells meaning the resting state. Yellow represents the initially triggered cell, while blue is the state of the cell that has been activated (computing state). The presented simulation results prove that the circuit successfully propagated the corresponding electrical signals by evolving the CA cells based on the provided mycelium branches in Table III.

The FUNGATERIA project has received funding from the European Union’s HORIZON-EIC-2021-PATHFINDER CHALLENGES programme under grant agreement No. 101071145

Co-funded by the European Union

European Innovation Council

Fungateria

5 Conclusions

In conclusion, the successful design of a digital twin for Engineered Living Materials (ELMs) necessitates a modeling framework that integrates seamlessly with hardware and fully utilizes available resources. Cellular Automata (CAs) have proven to be an excellent choice for this purpose, thanks to their capacity for simulating complex systems with scalability, modularity, and extensive parallelism. Employed specifically to map out reaction-diffusion processes, CAs facilitate a dynamic representation of both electrical and morphological activities of ELMs, ensuring the capture of their behavior with high fidelity. The effective implementation of this hardware-compatible modeling framework on a Field-Programmable Gate Array (FPGA) has led to the development of a prototype. This prototype, enhanced with custom circuits, adeptly emulates the initial electrical and morphological activities of the ELMs, demonstrating the potential and efficacy of this approach.

More specifically, this deliverable introduces a mycelium-based ELM model, utilizing CA within its framework. The model is grounded in reaction-diffusion processes, which are prevalent in natural systems, providing enhanced insights into the dynamics of such organisms through realistic simulations. It employs an activator-suppressor mechanism, capable of generating a diverse array of patterns and it extends to three dimensions based on the diffusion principle. Overall, the model effectively replicates the fundamental mechanisms of mycelium, including tip extension, branching, anastomosis, and nutrient uptake and it also exhibits characteristic bio-inspired patterns. The model alternates between different neighborhood weights in its diffusion processes, to capture the ELM's essence, which includes a condensed central biomass and discernible tips at its edges. Both 2D and 3D simulation results reflect the pattern observed in the biological fungi, validating the results of the proposed reaction-diffusion CA model.

In addition, a digital twin of a mycelium-based Engineered Living Material (ELM) within a Field-Programmable Gate Array (FPGA) has been successfully implemented. The implementation shows a significant speed boost and enhanced energy efficiency compared to basic software execution. This provides an ideal framework for simulating such biological organisms. This development marks a step forward in the simulation and understanding of mycelium-based materials within a controlled digital twin environment. It is important to note that the current implementation primarily focuses on simulating and observing the behavior of the ELM without the capacity for interactive feedback between the biological and digital systems, which will be investigated in future deliverables.

At the same time, a novel methodology for simulating ELMs is presented, focusing particularly on fungal mycelium as a promising candidate for developing next-generation materials. The core concept lies in modeling mycelium behavior, advocating for the use of digital twins to offer a comprehensive understanding of its complex dynamics. A novel approach is introduced through the implementation of Memristive Oscillating Cellular Automaton (MOCA), utilizing memristive nanoelectronic circuits to simulate the evolution of biological mycelium hyphae. The MOCA design incorporates a unipolar memristor device and exhibits three distinct operational phases: resting, activation, and suppression.

The FUNGATERIA project has received funding from the European Union's HORIZON-EIC-2021-PATHFINDER CHALLENGES programme under grant agreement No. 101071145

Co-funded by the European Union

European Innovation Council

Fungateria

These phases incorporate the reaction-diffusion dynamics observed in biological systems, enabling the simulation of mycelium growth and branching patterns. The simulation results demonstrate the successful propagation of activation signals across the MOCA grid, mimicking the tip growth and branching observed in fungal mycelium, showcasing the potential of this method in understanding the intricate behaviors of ELMs. The domino effect of neighboring cell activation reflects the biological communication pathways within the mycelium. Furthermore, the suppression phase effectively restricts uncontrolled growth, ensuring realistic behavior based on reaction–diffusion systems. This work paves the way for further advancements in the field of ELMs by offering a novel modeling approach using nanoelectronic memristive circuits that bridge the gap between traditional materials and living systems.

The FUNGATERIA project has received funding from the European Union's HORIZON-EIC-2021-PATHFINDER CHALLENGES programme under grant agreement No. 101071145

Co-funded by the European Union

European Innovation Council

Fungateria

Appx. I Related work

[A] I. K. Chatzipaschalis, T. P. Chatzinikolaou, I.-A. Fyrigos, A. Adamatzky, A. Rubio and G. C. Sirakoulis, "Memristor-Based Cellular Automata for Natural Language Processing," in *2023 30th IEEE International Conference on Electronics, Circuits and Systems (ICECS)*, 2023. ***(DOI: 10.1109/ICECS58634.2023.10382931)***

[B] T. P. Chatzinikolaou, I. K. Chatzipaschalis, E. Stavroulakis, E. Tsipas, I.-A. Fyrigos, A. Rubio and G. C. Sirakoulis, "Variability Tolerance Analysis of Memristive Wave Cellular Automata," in *2024 IEEE International Symposium on Circuits and Systems (ISCAS)*, 2024. ***(DOI: 10.1109/ISCAS58744.2024.10558112)***

[C] T. P. Chatzinikolaou, I. Tompris, I. K. Chatzipaschalis, I.-A. Fyrigos, M.-A. Tsompanas, A. Adamatzky and G. C. Sirakoulis, "Mycelium-based ELM Emulation Utilizing Memristive Oscillating Cellular Automata," in *2024 IEEE 24th International Conference on Nanotechnology (NANO)*, 2024. ***(accepted)***

[D] I. Tompris, I. K. Chatzipaschalis, T. P. Chatzinikolaou, I.-A. Fyrigos, M.-A. Tsompanas, A. Adamatzky, P. Ayes and G. C. Sirakoulis, "A Reaction-Diffusion Cellular Automata Model for Mycelium-based Engineered Living Materials Evolution", in *16th International Conference on Cellular Automata for Research and Industry (ACRI)*, 2024. ***(accepted)***

[E] I. K. Chatzipaschalis, I. Tompris, K. Rallis, T. P. Chatzinikolaou, I.-A. Fyrigos, M.-A. Tsompanas, A. Adamatzky, P. Ayes, A. Rubio and G. C. Sirakoulis, "Mycelium-based ELM Digital Twin Implemented in FPGA," in *16th International Conference on Cellular Automata for Research and Industry (ACRI)*, 2024. ***(accepted)***

The FUNGATERIA project has received funding from the European Union's HORIZON-EIC-2021-PATHFINDER CHALLENGES programme under grant agreement No. 101071145

Co-funded by the European Union

European Innovation Council

Fungateria

Appx. II References

[1] A. Mora-Boza, S. Acosta and M. Puertas-Bartolomé, "Chapter 9 - Biopolymers for the development of living materials for biomedical applications," in *Biopolymers*, V. Sessini, S. Ghosh and M. E. G. Mosquera, Eds., Elsevier, 2023, p. 263–294.

[2] S. C. Watkinson, L. Boddy and N. Money, The fungi, Academic Press, 2015.

[3] S. Liu and W. Xu, "Engineered Living Materials-Based Sensing and Actuation," *Frontiers in Sensors,* vol. 1, 2020.

[4] M. E. Antinori, M. Contardi, G. Suarato, A. Armirotti, R. Bertorelli, G. Mancini, D. Debellis and A. Athanassiou, "Advanced mycelium materials as potential self-growing biomedical scaffolds," *Scientific Reports,* vol. 11, p. 12630, 16 June 2021.

[5] A. Rodrigo-Navarro, S. Sankaran, M. J. Dalby, A. del Campo and M. Salmeron-Sanchez, "Engineered living biomaterials," *Nature Reviews Materials,* vol. 6, p. 1175–1190, 2021.

[6] A. Heide, P. Wiebe, L. Sabantina and A. Ehrmann, "Suitability of Mycelium-Reinforced Nanofiber Mats for Filtration of Different Dyes," *Polymers,* vol. 15, 2023.

[7] R. Omer, M. Z. Mohsin, A. Mohsin, B. S. Mushtaq, X. Huang, M. Guo, Y. Zhuang and J. Huang, "Engineered bacteria-based living materials for biotherapeutic applications," *Frontiers in Bioengineering and Biotechnology,* vol. 10, p. 870675, 2022.

[8] P. Q. Nguyen, N.-M. D. Courchesne, A. Duraj-Thatte, P. Praveschotinunt and N. S. Joshi, "Engineered living materials: prospects and challenges for using biological systems to direct the assembly of smart materials," *Advanced Materials,* vol. 30, p. 1704847, 2018.

[9] G. V. Angelova, M. S. Brazkova and A. I. Krastanov, "Renewable mycelium based composite – sustainable approach for lignocellulose waste recovery and alternative to synthetic materials – a review," *Zeitschrift für Naturforschung C,* vol. 76, p. 431–442, 2021.

[10] N. Attias, O. Danai, N. Ezov, E. Tarazi and Y. J. Grobman, "Developing novel applications of mycelium based bio-composite materials for design and architecture," *Proceedings of building with biobased materials: best practice and performance specification,* vol. 1, 2017.

The FUNGATERIA project has received funding from the European Union's HORIZON-EIC-2021-PATHFINDER CHALLENGES programme under grant agreement No. 101071145

Co-funded by the European Union

European Innovation Council

Fungateria

[11] S. Manan, M. W. Ullah, M. Ul-Islam, O. M. Atta and G. Yang, "Synthesis and applications of fungal mycelium-based advanced functional materials," *Journal of Bioresources and Bioproducts,* vol. 6, p. 1–10, 2021.

[12] A. Adamatzky, P. Ayres, A. E. Beasley, N. Roberts and H. A. B. Wösten, "Logics in fungal mycelium networks," *Logica Universalis,* vol. 16, p. 655–669, 2022.

[13] M. S. Fischer and N. L. Glass, "Communicate and Fuse: How Filamentous Fungi Establish and Maintain an Interconnected Mycelial Network," *Frontiers in Microbiology,* vol. 10, 2019.

[14] M. D. Fricker, L. L. M. Heaton, N. S. Jones and L. Boddy, "The mycelium as a network," *The fungal kingdom,* p. 335–367, 2017.

[15] F. A. Davidson, B. D. Sleeman, A. D. M. Rayner, J. W. Crawford and K. Ritz, "Large-scale behavior of fungal mycelia," *Mathematical and Computer Modelling,* vol. 24, p. 81–87, 1996.

[16] C. M. Regalado, J. W. Crawford, K. Ritz and B. D. Sleeman, "The origins of spatial heterogeneity in vegetative mycelia: a reaction-diffusion model," *Mycological Research,* vol. 100, p. 1473–1480, 1996.

[17] M. Ahangaran, N. Taghizadeh and H. Beigy, "Associative cellular learning automata and its applications," *Applied Soft Computing,* vol. 53, p. 1–18, 2017.

[18] J. V. Neumann, Theory of Self-Reproducing Automata, University of Illinois Press, 1966.

[19] S. Wolfram, Cellular automata and complexity: collected papers, crc Press, 2018.

[20] T. P. Chatzinikolaou, I.-A. Fyrigos, V. Ntinas, S. Kitsios, P. Bousoulas, M.-A. Tsompanas, D. Tsoukalas, A. Adamatzky and G. C. Sirakoulis, "Wave cellular automata for computing applications," in *2022 IEEE International Symposium on Circuits and Systems (ISCAS)*, 2022.

[21] I. K. Chatzipaschalis, T. P. Chatzinikolaou, I.-A. Fyrigos, A. Adamatzky, A. Rubio and G. C. Sirakoulis, "Memristor-Based Cellular Automata for Natural Language Processing," in *2023 30th IEEE International Conference on Electronics, Circuits and Systems (ICECS)*, 2023.

[22] I. A. Udugama, P. C. Lopez, C. L. Gargalo, X. Li, C. Bayer and K. V. Gernaey, "Digital Twin in biomanufacturing: challenges and opportunities towards its implementation," *Systems Microbiology and Biomanufacturing,* vol. 1, pp. 257-274, 01 July 2021.

[23] F. Tao, B. Xiao, Q. Qi, J. Cheng and P. Ji, "Digital twin modeling," *Journal of Manufacturing Systems,* vol. 64, pp. 372-389, 2022.

[24] D. Jones, C. Snider, A. Nassehi, J. Yon and B. Hicks, "Characterising the Digital Twin: A systematic literature review," *CIRP journal of manufacturing science and technology,* vol. 29, p. 36–52, 2020.

The FUNGATERIA project has received funding from the European Union's HORIZON-EIC-2021-PATHFINDER CHALLENGES programme under grant agreement No. 101071145

Co-funded by the European Union

European Innovation Council

Fungateria

[25] G. P. Boswell, H. Jacobs, K. Ritz, G. M. Gadd and F. A. Davidson, "The development of fungal networks in complex environments," *Bulletin of Mathematical Biology,* vol. 69, p. 605–634, 2007.

[26] L. Chua, "Memristor-the missing circuit element," *IEEE Transactions on Circuit Theory,* vol. 18, p. 507–519, 1971.

[27] D. B. Strukov, G. S. Snider, D. R. Stewart and R. S. Williams, "The missing memristor found," *nature,* vol. 453, p. 80–83, 2008.

[28] E. Tsipas, T. P. Chatzinikolaou, K.-A. Tsakalos, K. Rallis, R.-E. Karamani, I.-A. Fyrigos, S. Kitsios, P. Bousoulas, D. Tsoukalas and G. C. Sirakoulis, "Unconventional Computing With Memristive Nanocircuits," *IEEE Nanotechnology Magazine,* vol. 16, p. 22–33, 2022.

[29] R.-E. Karamani, I.-A. Fyrigos, V. Ntinas, I. Vourkas, A. Adamatzky and G. C. Sirakoulis, "Memristors in Cellular-Automata-Based Computing: A Review," *Electronics,* vol. 12, p. 3523, 2023.

[30] I. K. Chatzipaschalis, K.-A. Tsakalos, G. C. Sirakoulis and A. Rubio, "Parkinson's Treatment Emulation Using Asynchronous Cellular Neural Networks," in *2023 IEEE 14th Latin America Symposium on Circuits and Systems (LASCAS)*, 2023.

[31] T. P. Chatzinikolaou, I. K. Chatzipaschalis, K.-A. Tsakalos, R.-E. Karamani, I.-A. Fyrigos, S. Kitsios, P. Bousoulas, D. Tsoukalas and G. C. Sirakoulis, "Recognition of Greek Alphabet Characters with Memristive Neuromorphic Circuit," in *2023 IEEE International Conference on Metrology for eXtended Reality, Artificial Intelligence and Neural Engineering (MetroXRAINE)*, 2023.

[32] N. I. Dourvas, G. C. Sirakoulis and A. I. Adamatzky, "Parallel accelerated virtual physarum lab based on cellular automata agents," *IEEE Access,* vol. 7, p. 98306–98318, 2019.

[33] G. P. Boswell and S. Hopkins, "Linking hyphal growth to colony dynamics: spatially explicit models of mycelia," *Fungal Ecology,* vol. 1, p. 143–154, 2008.

[34] K. Sugimura, K. Shimono, T. Uemura and A. Mochizuki, "Self-organizing Mechanism for Development of Space-filling Neuronal Dendrites," *PLOS Computational Biology,* vol. 3, p. 1–12, November 2007.

[35] A. N. Landge, B. M. Jordan, X. Diego and P. Müller, "Pattern formation mechanisms of self-organizing reaction-diffusion systems," *Developmental biology,* vol. 460, p. 2–11, 2020.

[36] S. Kondo and T. Miura, "Reaction-diffusion model as a framework for understanding biological pattern formation," *science,* vol. 329, p. 1616–1620, 2010.

[37] K. Keren, "Cell motility: the integrating role of the plasma membrane," *European Biophysics Journal,* vol. 40, p. 1013–1027, 2011.

The FUNGATERIA project has received funding from the European Union's HORIZON-EIC-2021-PATHFINDER CHALLENGES programme under grant agreement No. 101071145

Co-funded by the European Union

European Innovation Council

Fungateria

[38] H. Kong, H. C. Akakin and S. E. Sarma, "A Generalized Laplacian of Gaussian Filter for Blob Detection and Its Applications," *IEEE Transactions on Cybernetics,* vol. 43, pp. 1719-1733, 2013.

[39] R. Krull, C. Cordes, H. Horn, I. Kampen, A. Kwade, T. R. Neu and B. Nörtemann, "Morphology of filamentous fungi: linking cellular biology to process engineering using Aspergillus niger," *Adv Biochem Eng Biotechnol,* vol. 121, p. 1–21, 2010.

[40] R. C. O'Reilly and J. M. Beck, "A family of large-stencil discrete Laplacian approximations in three-dimensions," *Int. J. Numer. Methods Eng,* p. 1–16, 2006.

[41] R. A. Van Gorder, "A theory of pattern formation for reaction–diffusion systems on temporal networks," *Proceedings of the Royal Society A: Mathematical, Physical and Engineering Sciences,* vol. 477, p. 20200753, 2021.

[42] G. P. Boswell, "Modelling mycelial networks in structured environments," *Mycological Research,* vol. 112, pp. 1015-1025, 2008.

[43] N. Dourvas, M.-A. Tsompanas, G. C. Sirakoulis and P. Tsalides, "Hardware acceleration of cellular automata physarum polycephalum model," *Parallel Processing Letters,* vol. 25, p. 1540006, 2015.

[44] D. D. Gajski, N. D. Dutt, A. C. H. Wu and S. Y. L. Lin, High—Level Synthesis: Introduction to Chip and System Design, Springer Science & Business Media, 2012.

[45] G. C. Sirakoulis, "Cellular Automata Hardware Implementation," in *Encyclopedia of Complexity and Systems Science*, R. A. Meyers, Ed., Berlin, Heidelberg: Springer Berlin Heidelberg, 2018, p. 1–29.

[46] A. Adamatzky and L. Chua, "Memristive excitable automata: structural dynamics, phenomenology, localizations and conductive pathways," *Advances in applied self-organizing systems,* p. 379–398, 2013.

[47] A. Ascoli, R. Tetzlaff, S.-M. S. Kang and L. Chua, "System-theoretic methods for designing bio-inspired mem-computing memristor cellular nonlinear networks," *Frontiers in Nanotechnology,* vol. 3, p. 633026, 2021.

[48] M. N. Kozicki and H. J. Barnaby, "Conductive bridging random access memory–materials, devices and applications," *Semiconductor Science and Technology,* vol. 31, p. 113001, October 2016.

[49] I.-A. Fyrigos, T. P. Chatzinikolaou, V. Ntinas, S. Kitsios, P. Bousoulas, M.-A. Tsompanas, D. Tsoukalas, A. Adamatzky, A. Rubio and G. C. Sirakoulis, "Compact thermo-diffusion based physical memristor model," in *2022 IEEE International Symposium on Circuits and Systems (ISCAS)*, 2022.

The FUNGATERIA project has received funding from the European Union's HORIZON-EIC-2021-PATHFINDER CHALLENGES programme under grant agreement No. 101071145

Co-funded by the European Union

European Innovation Council

[50] V. Ntinas, I.-A. Fyrigos, G. C. Sirakoulis, A. Rubio, J. Martín-Martinez, R. Rodríguez and M. Nafría, "Noise-induced performance enhancement of variability-aware memristor networks," in *2019 26th IEEE International Conference on Electronics, Circuits and Systems (ICECS)*, 2019.

[51] Z. Chai, J. Ma, W. D. Zhang, B. Govoreanu, J. F. Zhang, Z. Ji and M. Jurczak, "Probing the critical region of conductive filament in nanoscale HfO 2 resistive-switching device by random telegraph signals," *IEEE Transactions on Electron Devices,* vol. 64, p. 4099–4105, 2017.

[52] L. B. Poehls, M. C. R. Fieback, S. Hoffmann-Eifert, T. Copetti, E. Brum, S. Menzel, S. Hamdioui and T. Gemmeke, "Review of manufacturing process defects and their effects on memristive devices," *Journal of electronic testing,* vol. 37, p. 427–437, 2021.

[53] A. Grossi, E. Nowak, C. Zambelli, C. Pellissier, S. Bernasconi, G. Cibrario, K. El Hajjam, R. Crochemore, J. F. Nodin, P. Olivo and L. Perniola, "Fundamental variability limits of filament-based RRAM," in *2016 IEEE International Electron Devices Meeting (IEDM)*, 2016.

[54] J. B. Roldán, E. Miranda, D. Maldonado, A. N. Mikhaylov, N. V. Agudov, A. A. Dubkov, M. N. Koryazhkina, M. B. González, M. A. Villena, S. Poblador, M. Saludes-Tapia, R. Picos, F. Jiménez-Molinos, S. G. Stavrinides, E. Salvador, F. J. Alonso, F. Campabadal, B. Spagnolo, M. Lanza and L. O. Chua, "Variability in Resistive Memories," *Advanced Intelligent Systems,* vol. 5, p. 2200338, 2023.

[55] W. Sun, B. Gao, M. Chi, Q. Xia, J. J. Yang, H. Qian and H. Wu, "Understanding memristive switching via in situ characterization and device modeling," *Nature communications,* vol. 10, p. 3453, 2019.

The FUNGATERIA project has received funding from the European Union's HORIZON-EIC-2021-PATHFINDER CHALLENGES programme under grant agreement No. 101071145

Co-funded by the European Union

European Innovation Council